REPORT DOCUMENTATION PAGE

Form Approved
OMB NO. 0704-0188

1. AGENCY USE ONLY (Leave Blank)	2. REPORT DATE	3. REPORT TYPE AND DATES COVERED
	JUNE 15, 2002	FINAL 31 JANUARY 2001 TO 15 JUNE 2002

4. TITLE AND SUBTITLE
BROADBAND FOCUSED RADAR AT GROUND PENETRATING FREQUENCIES FOR DETECTING MINES, UNEXPLODED ORDNANCE, OR MOBILITY RELATED SURFACE LAYERS

5. FUNDING NUMBERS
C DAAD19-01-C-0021

6. AUTHOR(S)
WOLLNY, W. TOM

7. PERFORMING ORGANIZATION NAME(S) AND ADDRESS(ES)
QUICK REACTION CORPORATION
2533 N. CARSON STREET SUITE 1608
CARSON CITY, NV 89706

8. PERFORMING ORGANIZATION
REPORT NUMBER QRC-64636-02

9. SPONSORING / MONITORING AGENCY NAME(S) AND ADDRESS(ES)
U. S. Army Research Office
ATTN: AMSRL-RO-RI
P.O. Box 12211
Research Triangle Park, NC 27709-2211

10. SPONSORING / MONITORING AGENCY REPORT NUMBER
42015.1-EV-SBI

11. SUPPLEMENTARY NOTES
The views, opinions and/or findings contained in this report are those of the author(s) and should not be construed as an official Department of the Army position, policy or decision, unless so designated by other documentation.

12 a. DISTRIBUTION / AVAILABILITY STATEMENT
Approved for public release; distribution unlimited.

12 b. DISTRIBUTION CODE

13. ABSTRACT (Maximum 200 words)

Report developed under SBIR Contract for topic Army 00-027 effort is to produce a fully mobile, broadband radar system with a focused planar beam over approximately 10 MHz to 1000 MHz for the detection of buried objects and the detection of frozen or thawed layers which effect mobility. The proposed antenna configuration consisted of a contra-wound helix, to cover the frequencies from 10 MHz to 100 MHz, and an array of contra-wound conical spirals, to cover the range from 100 MHz to 1000 MHz. A detailed near field analysis of the helix yielded the results that at lower frequencies the axial component of the electric field intensity (E_z) dominates the transverse components (E_x and E_y). The windings of a helix has a z component which gives rise to (E_z) component in the field. The z component also adds on the counter wound helix which makes this antenna solution unacceptable in the near field . It is clear that when the antenna aperture or elements are restricted to lie in a plane, then the *z* components from symmetric current components will cancel at observation points near the axis. Structures that satisfy this condition are a planar aperture with a TEM aperture field and planar wires (spirals). The major disadvantage is the large size and weight (approximately 75 by 54 by 70 inches for a horn that operates down to 100 MHz). A planar dual linear polarization sinuous antenna is selected to provide the desired frequency coverage. The low frequency cut off is determined by the largest circumference (diameter = 50 inches for 50 MHz @-12dBi). Larger diameters would provide lower frequency response. The radar is an Agilent network analyzer which is programmed to cover the frequency band supported by a Dell computer driving two displays.

14. SUBJECT TERMS	15. NUMBER OF PAGES
SBIR REPORT, GROUND PENETRATING RADAR, WIDE BAND ANTENNA, CONTRA-WOUND HELIX, SINUOUS ANTENNA	35
	16. PRICE CODE

17. SECURITY CLASSIFICATION OR REPORT	18. SECURITY CLASSIFICATION ON THIS PAGE	19. SECURITY CLASSIFICATION OF ABSTRACT	20. LIMITATION OF ABSTRACT
UNCLASSIFIED	UNCLASSIFIED	UNCLASSIFIED	UL

NSN 7540-01-280-5500

Standard Form 298 (Rev.2-89)
Prescribed by ANSI Std. 239-18
298-102

20021021 050

A Program Description

This is the final report on the Phase I SBIR A00-028 effort is to produce a fully mobile, broadband radar system with a focused planar beam over approximately 10 MHz to 1000 MHz for detection of frozen or thawed layers and the detection of buried objects.

The original proposed antenna configuration consists of a contra-wound helix to cover the frequencies from 10 MHz to 100 MHz and an array of contra-wound conical spirals to cover the range from 100 MHz to 1000 MHz. A conceptual drawing of the antenna system is shown in Figure 1. A two-by-two array of conical spirals is shown, but the final configuration will be determined by the outcome of tradeoff studies involving various design parameters. Performance issues that will be addressed include:

- polarization isolation,
- allowable physical size,
- uniformity of spot illumination (amplitude and phase), and
- input VSWR of the antennas

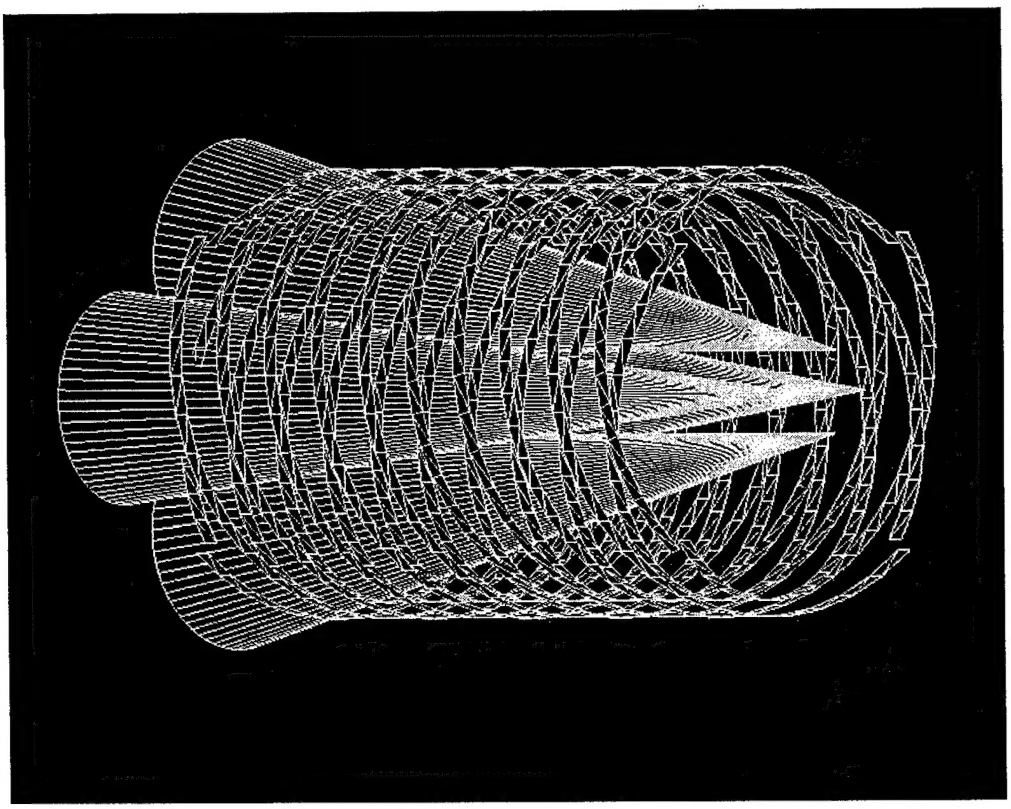

Figure 1: Broadband antenna system concept: an array of conical spirals for high band and a contra-wound quadrifilar helix for the low band.

B Introduction

Detection of subsurface targets is improved by the use of low frequencies, because low frequency waves penetrate moist ground more efficiently than high frequency waves. The research effort has focused on the helix antenna as a possible radiating structure capable of providing a compact illumination spot over the frequency band of 10 MHz to 100 MHz.

The parameters of the basic helix are illustrated in Figure 2. N is the number of turns, D the diameter, s the spacing between each turn and ℓ the arc length of each turn. The total length of the antenna is $L = Ns$, while the total arc length of the wire is $N\ell$. The pitch angle is defined as

$$\alpha = \tan^{-1}\left(\frac{s}{\pi D}\right) = \tan^{-1}\left(\frac{s}{C}\right)$$

where C is the circumference. The sense of the helix is defined using the right hand or left hand rule. For example, in Figure 2, if the thumb of the right hand is pointed in the direction of radiation (the positive z axis) then the fingers give the direction of the windings for increasing z. Therefore, the sense of the helix is referred to as right handed.

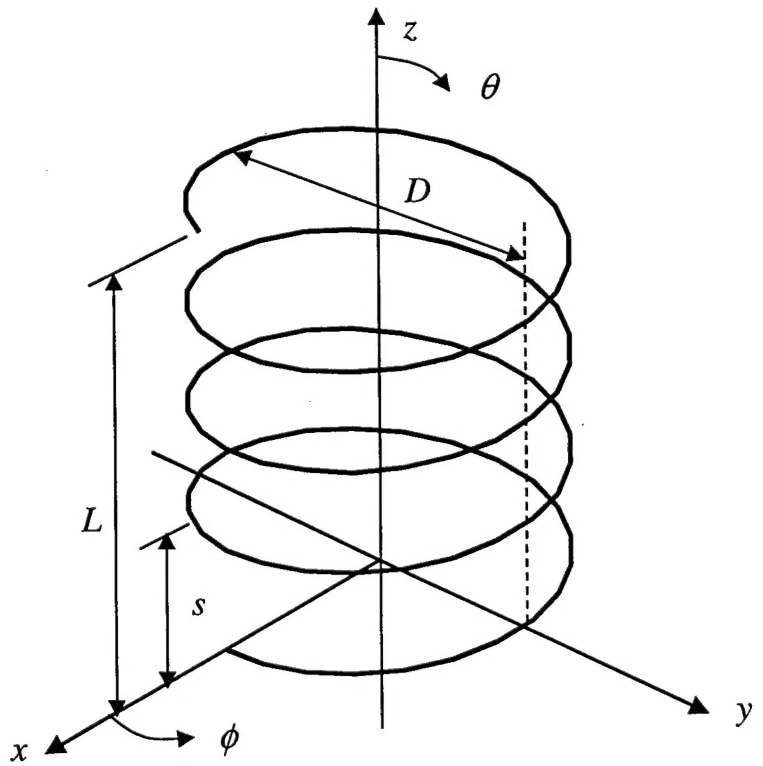

Figure 2: Definition of helix parameters.

The radiation characteristics of the helix were established by Kraus [1]. The characteristics can be varied by controlling the size of the geometrical parameters relative to the wavelength. With regard to the far-field, improved performance can be achieved by adding more helices (arms) and feeding them with the proper phase relationship as shown in Figure 3. Bifilar and quadrifilar helix antennas consist of two and four arms, respectively. One of the attractive features of the helix is its wide bandwidth. A simple helix can be made to operate over a couple of octaves. Bandwidths of 5:1 have been reported for the quadrifilar helix. Adding more arms also reduces the radiation in the back direction.

The polarization can range from linear to circular as the frequency is changed. Linear polarization can be assured by adding a second set of windings that are wound in a sense opposite that of the first set (a counter-wound helix antenna).

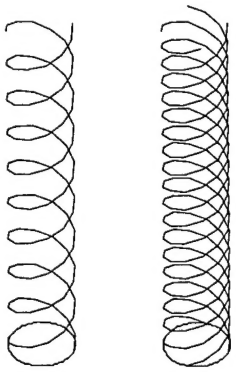

Bifilar Quadrifilar

Figure 3: Multiple filament helices.

Previous studies on optimizing the performance of the helix have been concerned with its far-field behavior [2]. In this particular application the near-field performance is our interest. For example, the quality of the far-field pattern of the helix is dependent on the ground plane size [3]. For near-field operation, however, the ground plane may not be a critical parameter.

In order to provide a compact illumination spot, the ground will be in the near field of the helix. The near field is characterized by the presence of a radial field component and fields that deviate from the $1/R$ spherical wave behavior that occurs in the far zone. This leads to phase and amplitude errors that degrade the resolution of images constructed from the received scattered field. However, these errors are predictable and potentially can be corrected in the processing of the received signal.

Our research examines the suitability of using counter-wound helix antennas for near-field imaging. The antenna was modeled using the method of moments technique, and the near fields calculated as a function of distance from the end of the helix. Several design parameters were varied to determine their effect on the near-field behavior. The fields of monofilar, bifilar, and quadrifilar contra-wound helices were examined. The

returns from several simple targets in free space were processed to determine the quality of the "down range" coordinate used to construct an image.

C Analysis Method

The method of moments (MM) was used to compute the radiation from the helix. The method of moments is a technique that converts the E-field integral equation (EFIE) to a set of simultaneous linear equations that can be solved using standard matrix methods. The EFIE is derived from Maxwell's equations and the boundary conditions. MM has become a standard analysis method and has been incorporated into many commercially available software codes. The technique is rigorous in the sense that if it is properly applied, the solution for the currents on the helix is sure to converge to the "correct" value.

The software package used in this work was an older code called *PATCH* [4]. The accuracy of *PATCH* has been validated for a wide range of antenna and scattering problems. First the antenna and any surrounding structures to be modeled are discretized into a triangular mesh. The MM code computes the current on all triangular facets (subdomains) simultaneously by solving a matrix equation. Therefore interactions between all currents on the body are included. Once the antenna currents have been determined, the radiation integrals [5] can be used to find the near and far fields.

The number of triangles determines the size of the matrix. For a converged solution the general rule of thumb is that the triangle edges should not exceed 0.1λ, where λ is the wavelength. Thus computer memory and processing time can limit the size of an antenna problem that can be analyzed in practice.

D Helix Antenna Design

D.1 Design issues

The antenna design problem can be broken into two tasks: (1) radiation field characteristics, and (2) input impedance control and matching. For the most part, the two problems can be approached independently. At this point the research focused on the first step: designing an antenna structure that provides the desired radiation properties over the frequency band of interest.

Most conventional helix design tradeoff formulas are based on far-field performance and, therefore, not directly applicable to the near-field problem. Exceptions are the formulas related to the input reflection coefficient (or, equivalently, the voltage standing wave ratio, VSWR). In free space (i.e., no nearby obstacles) a simple helix with a ground plane can be matched to provide a VSWR less than 3:1 over the range of circumferences $0.65 < C/\lambda < 1.7$ even though the radiation characteristics change dramatically over this range. This bandwidth can be increased by adding more arms or tapering the diameter, as demonstrated in references [6-8]. The above range of circumferences for matching the antenna input would seem to form a good starting point for sizing the helix. At 10 MHz this guideline would dictate a circumference of about

19m or diameter of about 6m. Clearly, this is prohibitive for the current application, and it is expected that a diameter of about 2m would be about the largest acceptable diameter. Furthermore, a length of 3 to 4m would probably be the longest that could be accommodated by a mobile system. Thus all of the helices considered in the study were less than 2m in diameter and 4m in length.

D.2 Far-field Patterns Single Helix

As a first step, the far-field radiation patterns for monofilar, bifilar and quadrifilar antennas were computed. Sample data for the helices shown in Figure 4 are given in Figures 5, 6 and 7 (a stand-alone helix, a helix with an infinite ground plane, and a helix with a finite ground plane). For each case, the patterns are normalized to the maximum field value. The helix diameter is 0.83m and the length 4m. The pitch angle is approximately 11 degrees and there are 4 turns.

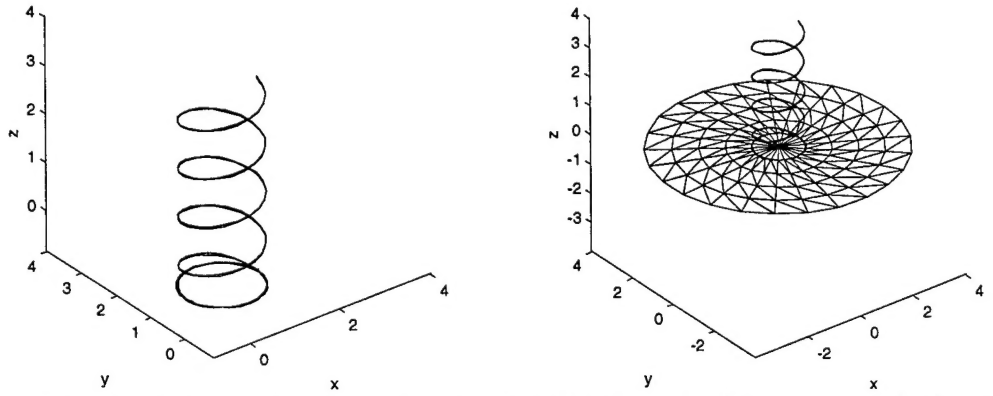

Figure 4: Stand alone helix with a base ring (left) and with a ground plane (right)

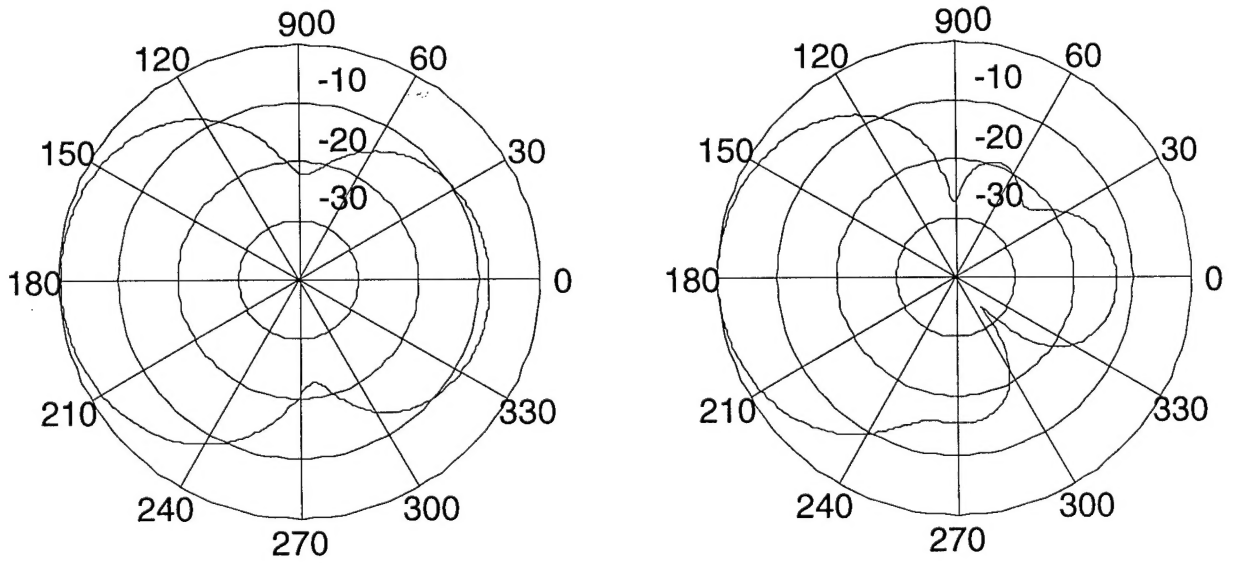

Figure 5: Radiation pattern of a "stand alone" helix with a base ring (50 MHz, E_θ left, E_ϕ right).

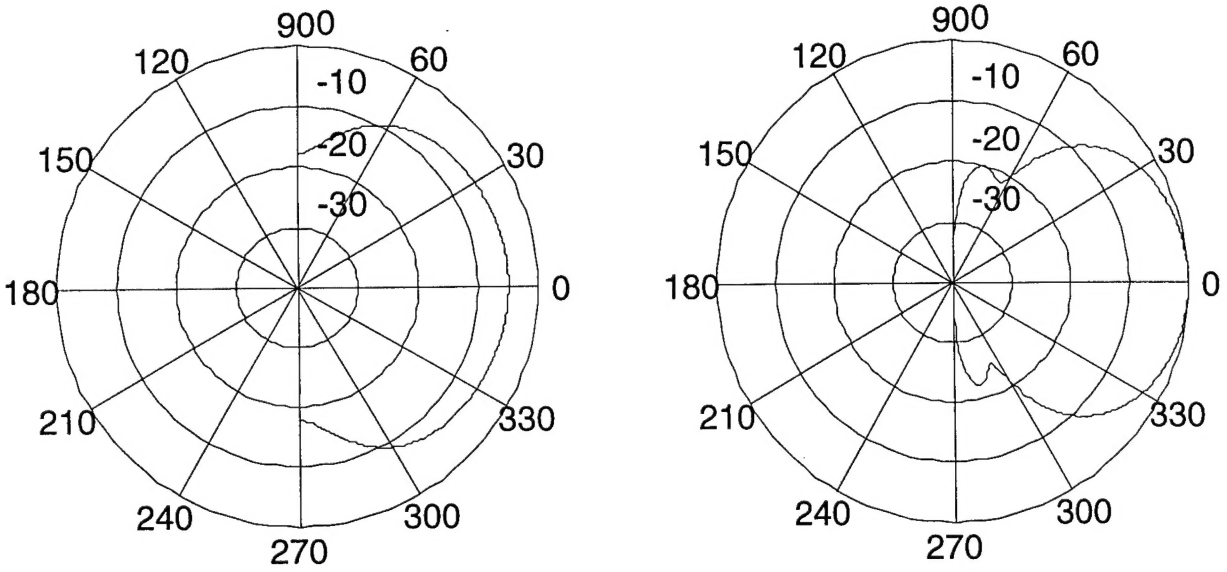

Figure 6: Radiation pattern of a helix over an infinite ground plane (50 MHz, E_θ left, E_ϕ right).

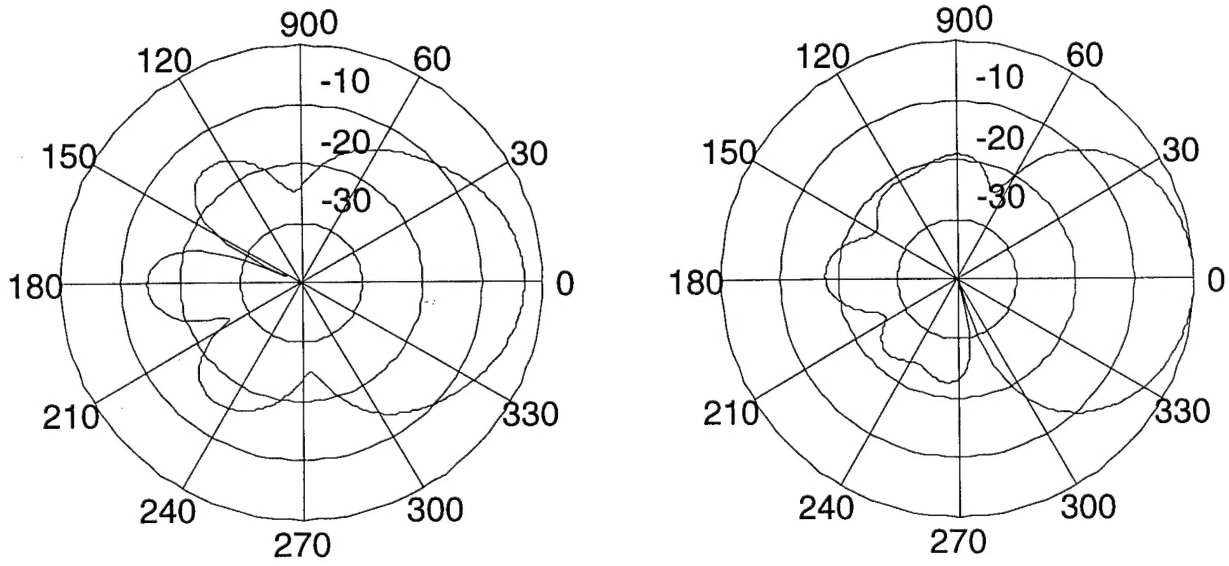

Figure 7: Radiation pattern of a helix over an finite ground plane (50 MHz, E_θ left, E_ϕ right).

The stand-alone helix actually has more radiation in the back direction. This is because the base ring radiates like a loop antenna. For an infinite ground plane, there is no radiation in the rear hemisphere. For a finite ground plane (a disk in this case) there is still significant radiation in the back direction; however, it is greatly reduced from the stand-alone helix. The polarization is circular, with relatively small axial ratios in the main beam direction.

E Near-field Distribution of the Single Helix

Near-field distributions of the helix are shown in Figures 8 and 9. Figure 8 contains plots of the magnitudes of the *x*, *y*, and *z* components of the electric field on the $z = 6$m plane as a function of *x* and *y* for a frequency of 10 MHz. The end of the helix winding is at $z = 4$m, and hence this plot depicts the field distribution 2m from the end of the antenna. The lower right hand plot is the magnitude of the total field, which is proportional to the total voltage received at the antenna terminals. (The antenna cannot distinguish the fraction of voltage due to the individual components.) All plots in the same figure are normalized to a common value.

Note that the *x* and *y* components are negligible compared to the *z* component, which is expected in the near field. The far-field limit is defined as the minimum distance at which the radial component of the radiation field has decayed to a negligible level, the wavefronts become spherical and the fields decay as $1/R$. (The radial distance R in a direction along the helix axis is equal to *z*.) The radial and non-$1/R$ components of the field are reactive. They affect the input impedance but do not contribute to the radiated power of the antenna.

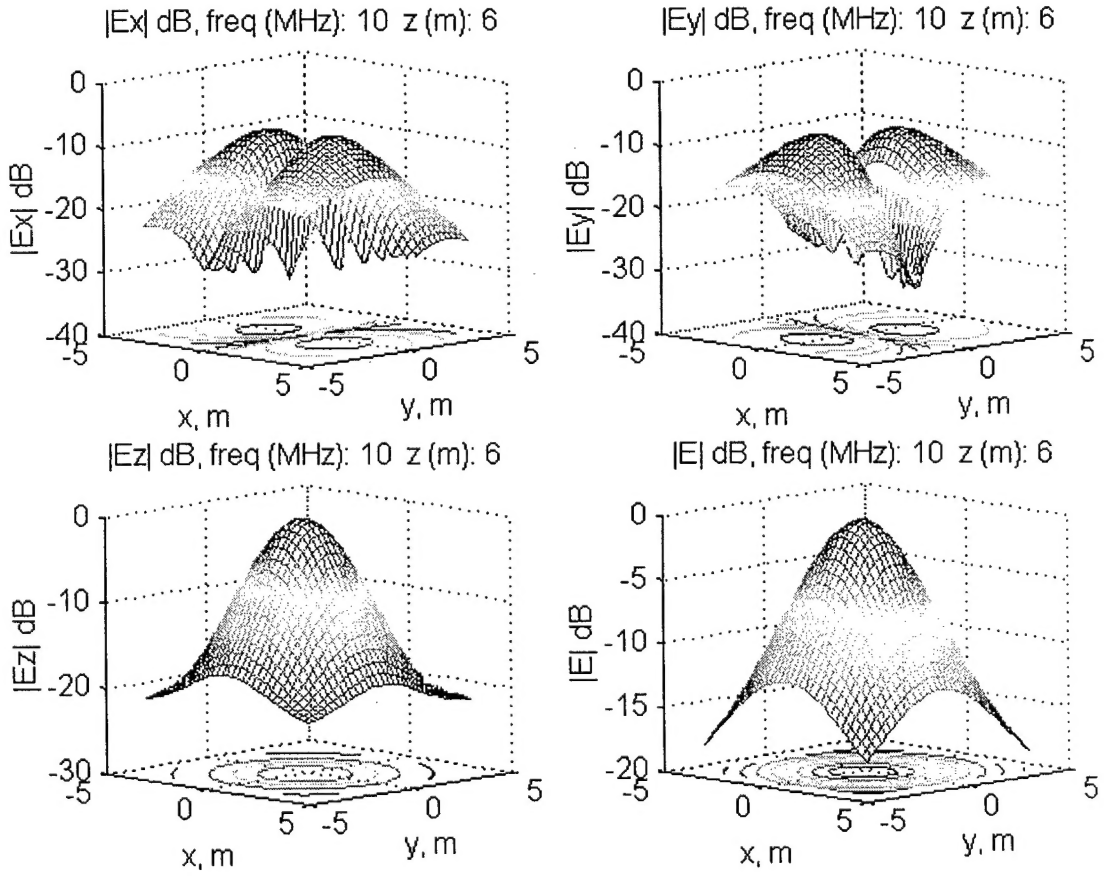

Figure 8: Near field distribution of the single helix for 10 MHz.

For aperture and wire antennas, the far-field distance is typically taken as $2L^2/\lambda$, where *L* is the length of the antenna. For the 4m helix above a ground plane, which makes the antenna 8m when the image is included, the near field would extend to about 4m at 10 MHz and 40m at 100 MHz. This is a common measure of the far field but has no physical significance; there is no abrupt change in the behavior of the fields at $2L^2/\lambda$. In fact, within the near field region the fields can vary radically as a function of angle at a fixed value of *R*. The radial component in one direction can be negligible, while that in another direction can be vary large.

In Figure 9 near-field data is plotted for 90 MHz. Note that the *z* component has already decayed to a negligible value and the antenna is essentially linearly polarized in the *y* direction. The *x* and *y* components are approximately equal, resulting in nearly circular polarization.

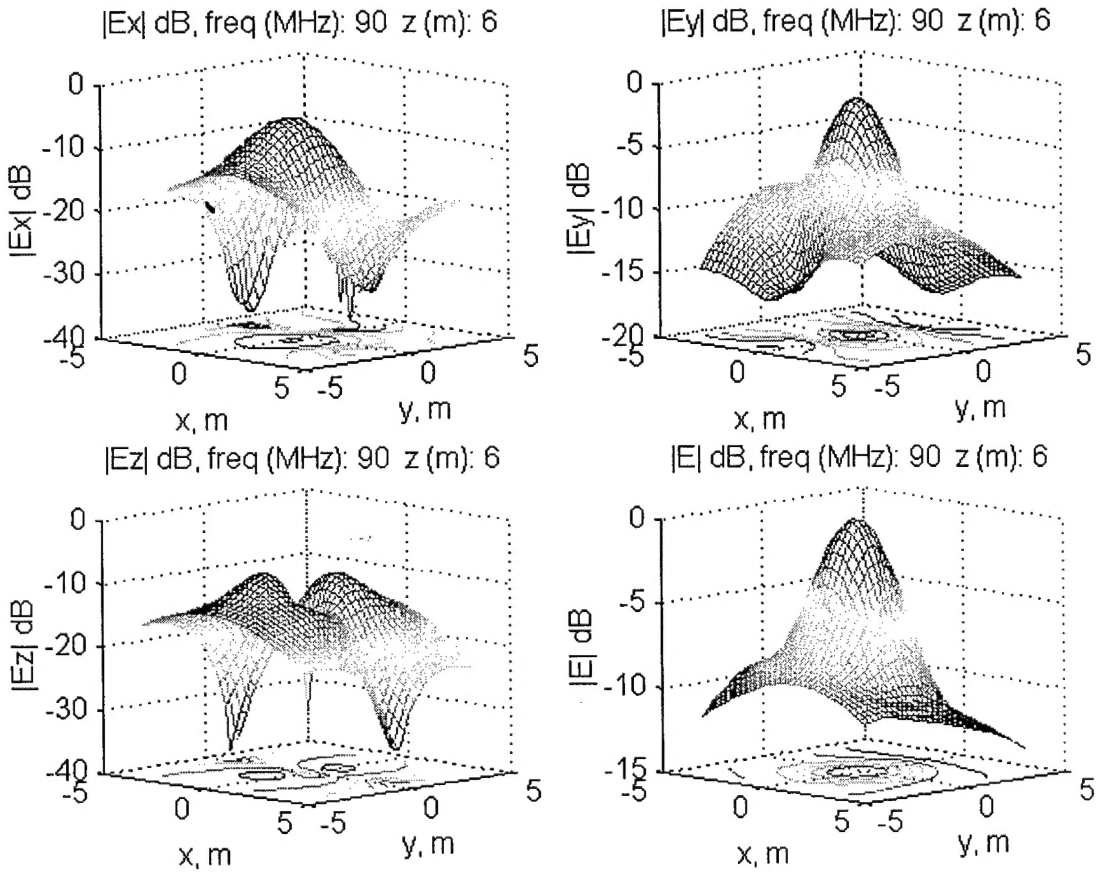

Figure 9: Near field distribution of the single helix for 90 MHz.

F Near-field Distribution of the Two-Arm Counter-wound Helix

For imaging applications linear polarization is desirable. Linear polarization in the far field can be obtained by adding a winding in the opposite sense for each arm in the

original helix. The simplest counter-wound helix consists of two windings: one left hand and the other right hand, as shown in Figure 10. The near-field distributions of the counter-wound helix at 10 MHz and 90 MHz are shown in Figures 11 and 12.

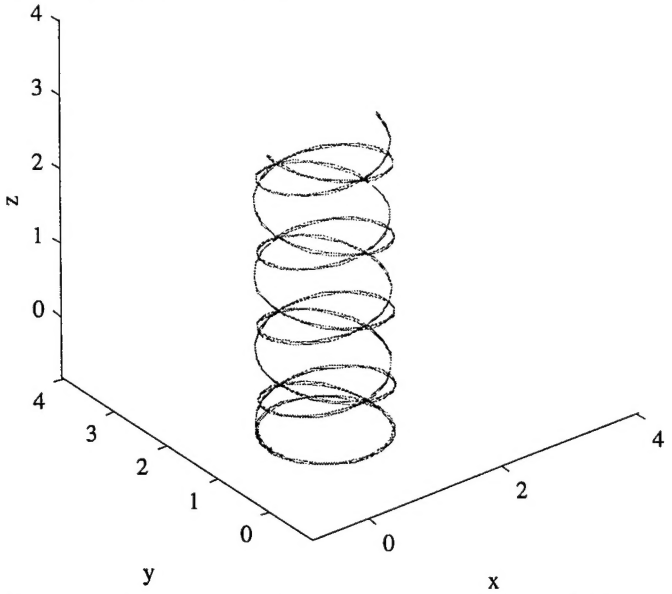

Figure 10: Counter-wound helix consisting of two windings

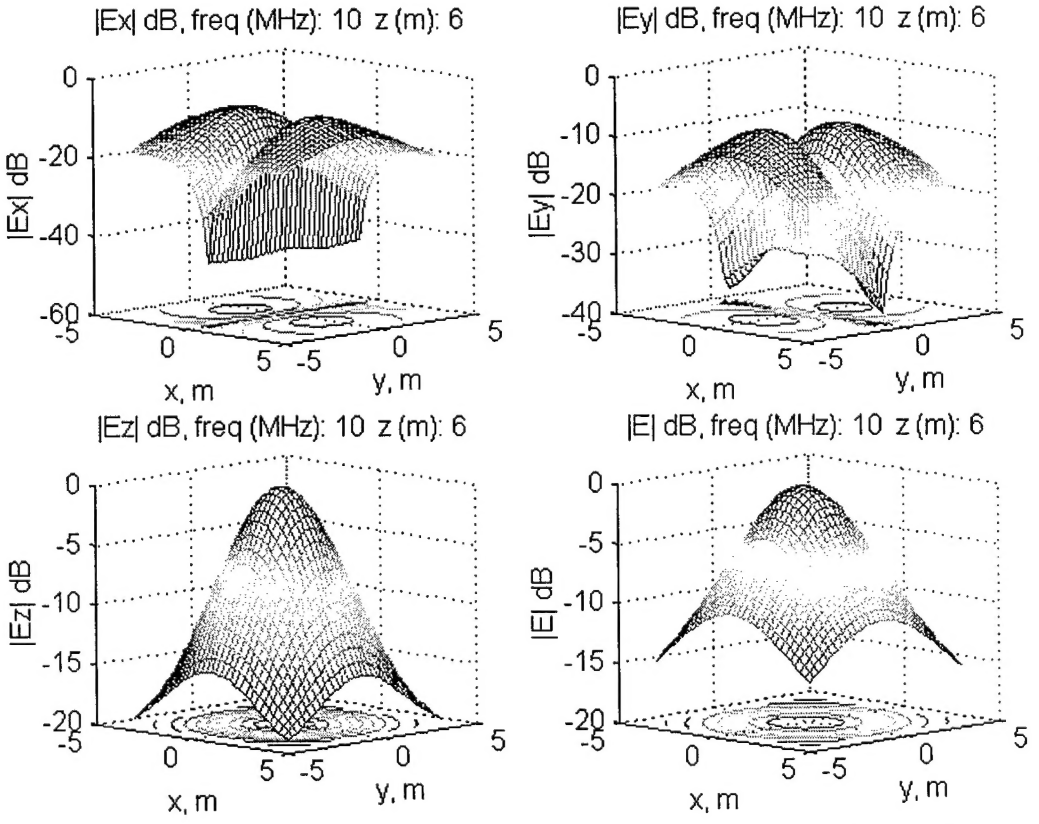

Figure 11: Near-field distribution of the single counter-wound helix for 10 MHz.

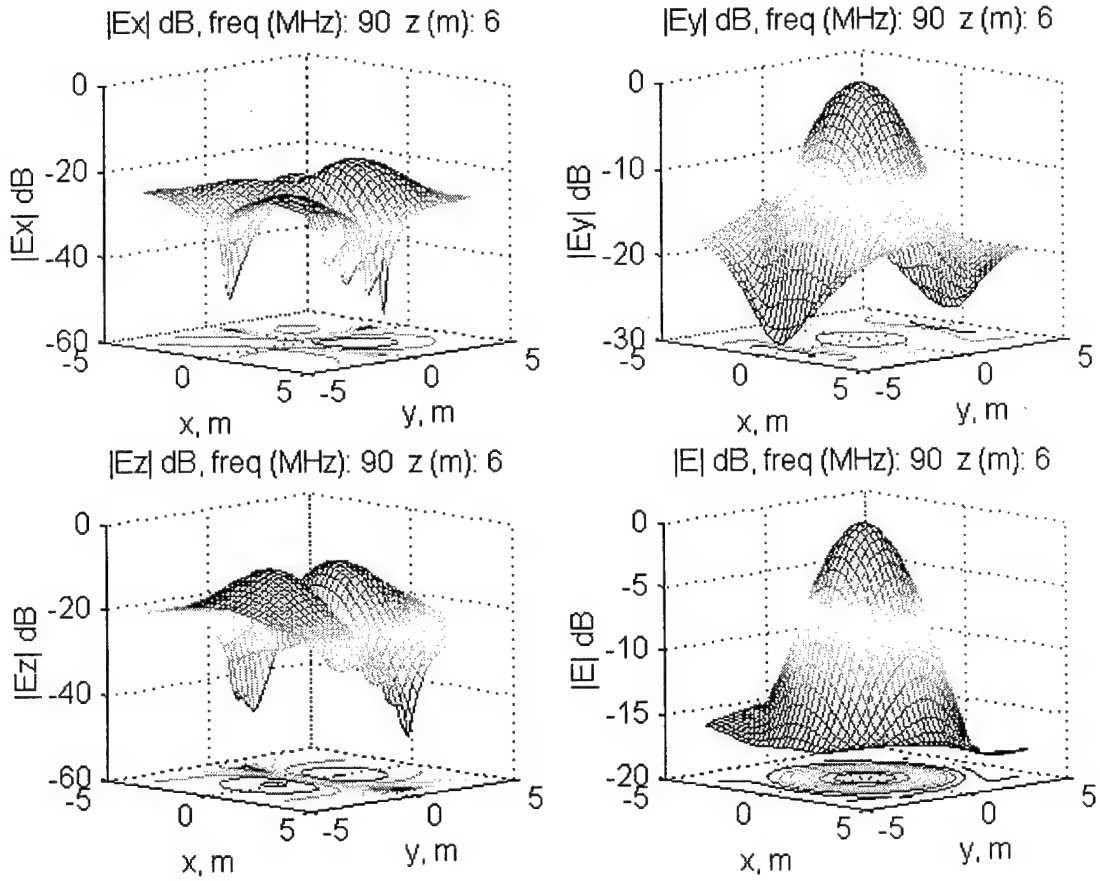

Figure 12: Near-field distribution of the single counter-wound helix for 90 MHz.

The magnitude of the total field provides a well-defined spot at all frequencies between 10 MHz and 100 MHz. However, at low frequencies the longitudinal (*z*) component dominates, whereas, at high frequencies the antenna becomes linearly polarized in the conventional sense, because the *y* component dominates. The near fields were calculated at distances out to 4m from the end of the helix, and the same behavior occurred at all distances.

G Fields of the Counter wound Bifilar Helix

In order to minimize weight and reduce the complexity of the microwave circuitry that will be needed to feed the helix elements, the smallest possible number of filaments is desired. Although the two-arm counter-wound helix provides the required spot illumination, it is expected that more arms may have to be added to: (1) reduce the radiation in the back direction, and (2) match the input impedance to the feed line. A counter-wound bifilar helix is shown in Figure 13, and the near fields at 10 MHz and 90 MHz are given in Figures 14 and 15. The illumination spots are not as circularly symmetric in this case, because the two additional arms have reduced the geometrical symmetry from left-right half space to quadrants.

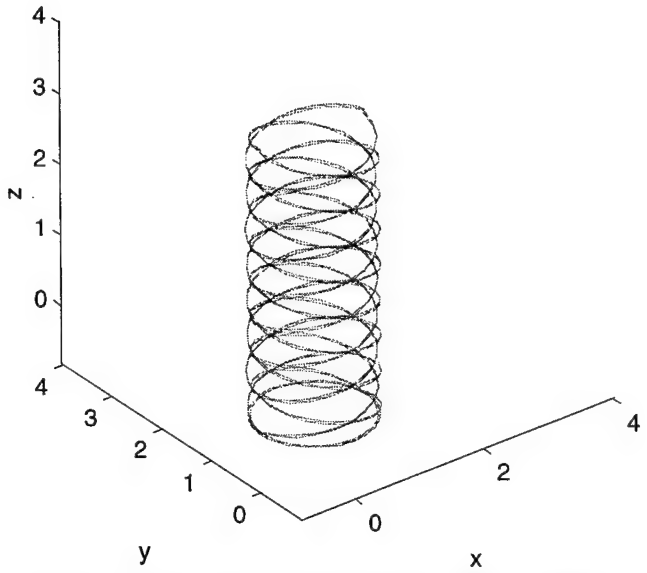

Figure 13: Counter wound bifilar helix.

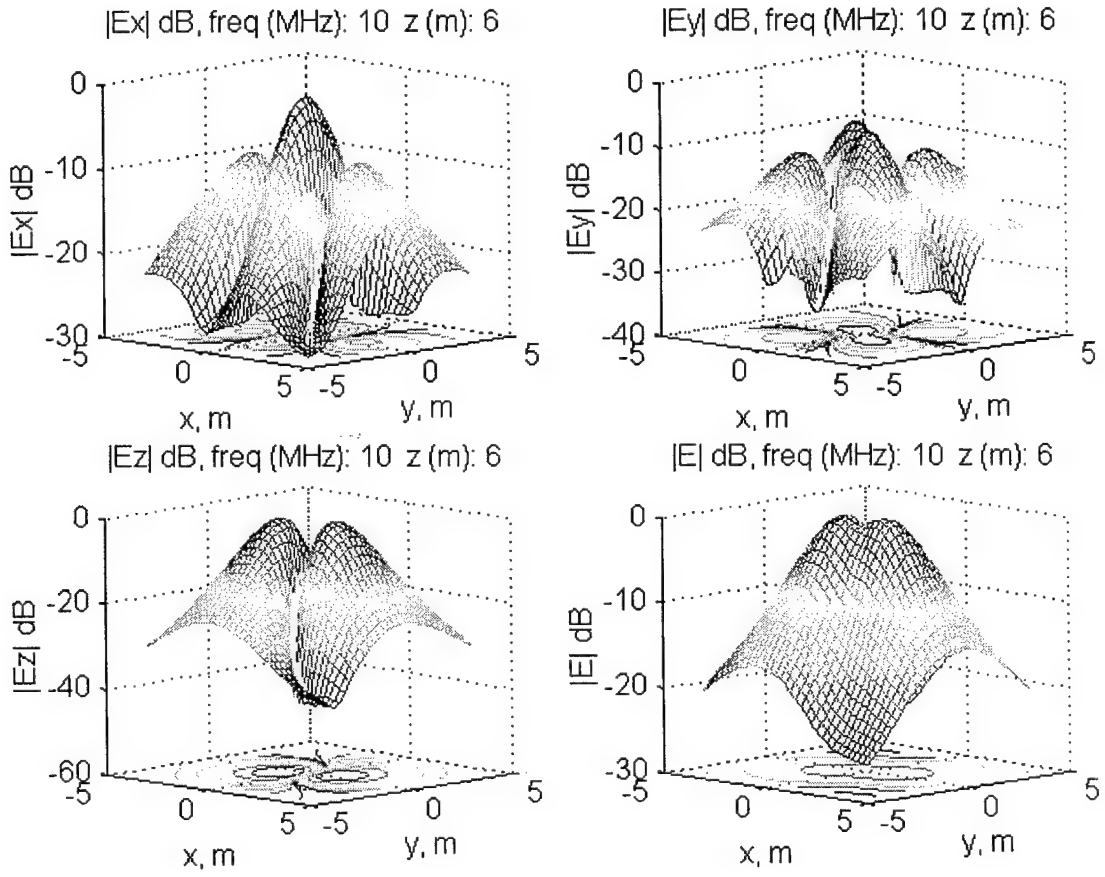

Figure 14: Near-fields of the counter wound bifilar helix at 10 MHz.

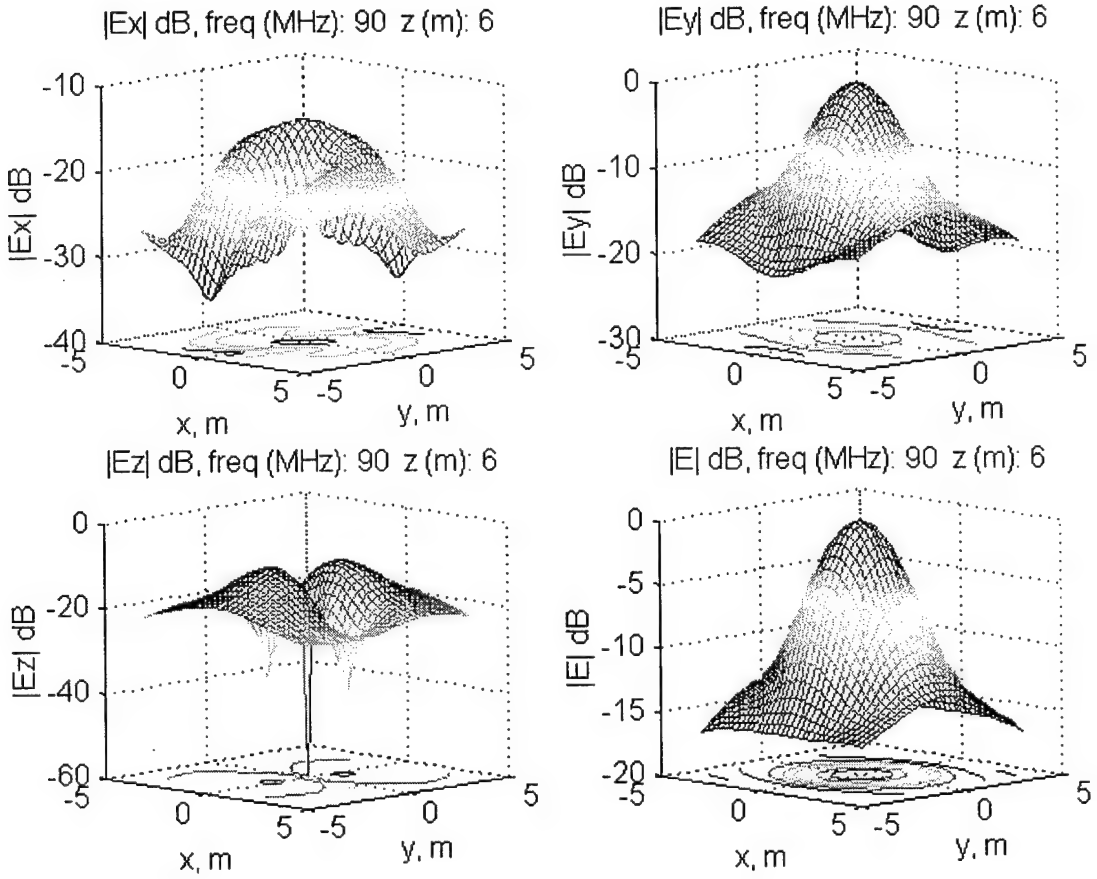

Figure 15: Near-fields of the counter wound bifilar helix at 10 MHz.

H Near-Field Imaging Issues

There are several problems that arise when imaging objects in the near field of the antenna. The first is that the antenna voltage is due to a mix of polarizations. Specifically, there is a large longitudinal component to the field vector. Second, because the targets are potentially in the near field of the antenna, there is not a well-defined outward propagating spherical wave impinging on the target. It is the measured time delay of the scattered spherical wave that typically provides the "down range" coordinate in the image. In fact, the presence of an obstacle in the near field is detected primarily by its interaction (or coupling) with the near fields.

Because of these special aspects of imaging objects in the near field, the returns from several objects in front of the antenna were processed to obtain the time response. The objects included a circular disk and *x* and *y* directed strips located at various distances from the end of the antenna. Figure 16 shows the helix and disk. Free space was assumed. The voltage at the antenna terminals was computed at 64 equally spaced frequencies from 10 MHz to 100 MHz with the disk present and then subtracted from the voltages that were computed at the same frequencies when no disk was present. An inverse fast Fourier transform (IFFT) was taken of the difference.

Figure 17 shows the terminal voltage (in dB) as a function of frequency with and without the disk. The same terminal voltage is applied in both cases, so the levels of the two curves can be compared. The IFFT of the residual is shown in Figure 18. All 64 frequencies are used in the IFFT. Note that the residual returns are about 50 dB down from the "raw" voltages.

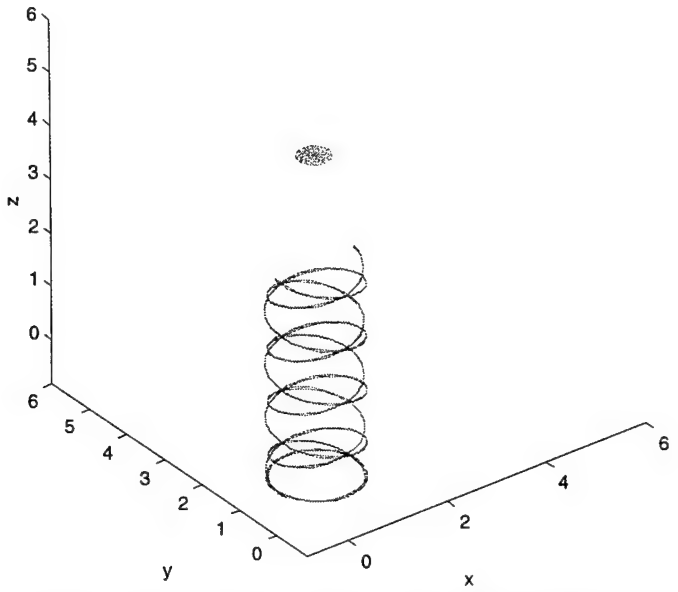

Figure 16: Counter-wound helix with a scattering disk located in front.

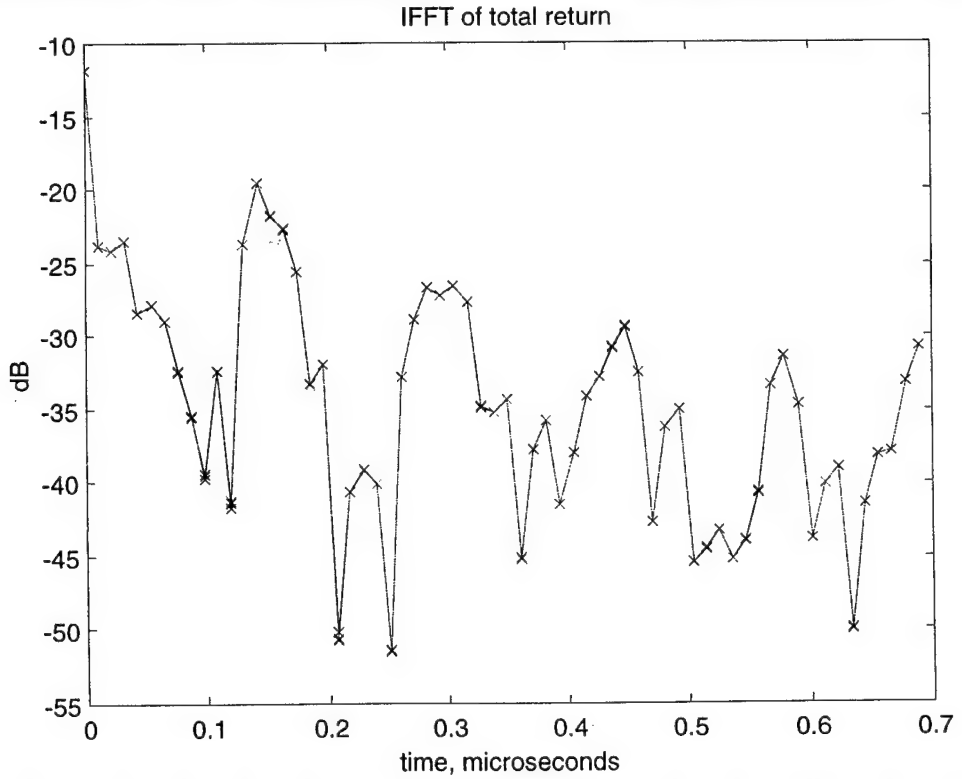

Figure 17: Terminal voltages with and without the scattering disk (disk at 6m).

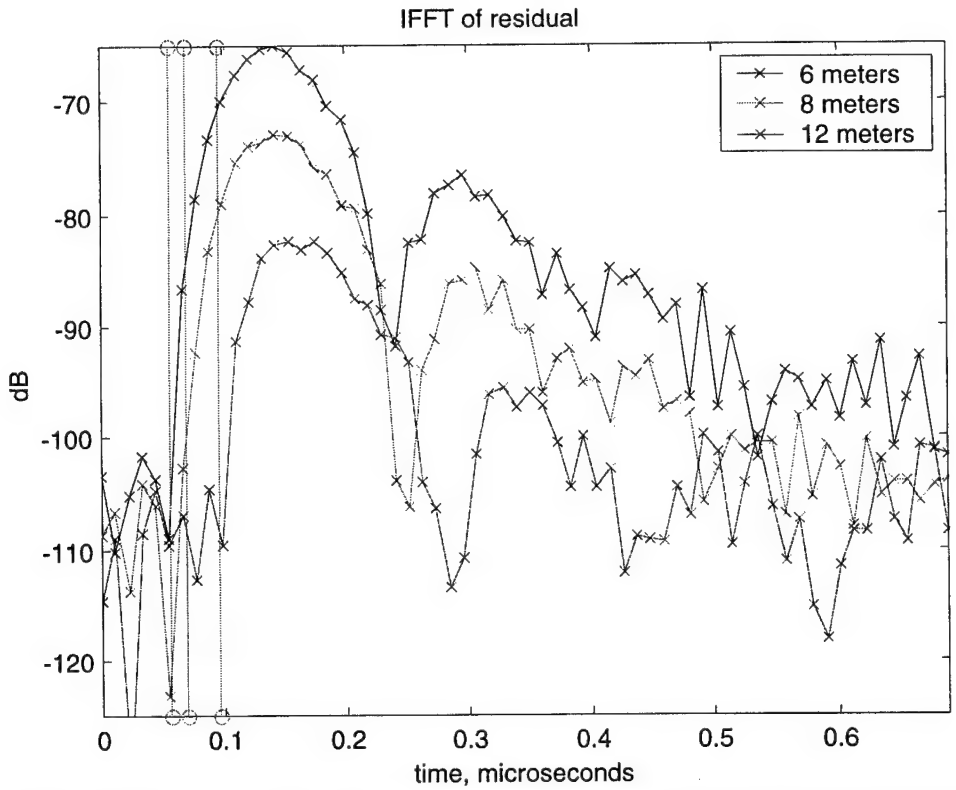

Figure 18: Full band IFFT of the residual voltages for the disk at three different distances.

The spacing of the vertical lines in Figure 18 are for the time delay differences that would occur if the disk were illuminated by a plane wave (although they have been shifted by a constant). It is evident that the time delay difference in the returns from the disk correspond closely to those expected for plane wave scattering.

The polarization selectivity was examined by calculating the scattering from thin strips oriented in the x and y directions. Figures 19 and 20 show the IFFTs of the raw and residual returns, respectively, for a x-directed strip. Figures 21 and 22 show the corresponding data for a y directed strip. There is a much stronger return for the y strip (almost 40 dB) because the antenna polarization tends to this direction at the high frequencies in the band.

In order to examine the effect of bandwidth, the IFFT was performed using only the 32 frequencies in the upper half of the 10 to 100 MHz band. The results are shown in Figures 23 and 24. Note that the IFFT of the residuals is close to that of the full band (Figure 18). This might lead one to conclude that the lower half of the frequency band is not needed, thereby allowing a narrower band antenna to be used. However, this simple example does not take into account the frequency dependence of the ground transmission and reflection coefficients. The frequencies in the upper half of the band would suffer more attenuation, and the lower band frequencies would play a more important role in the imaging.

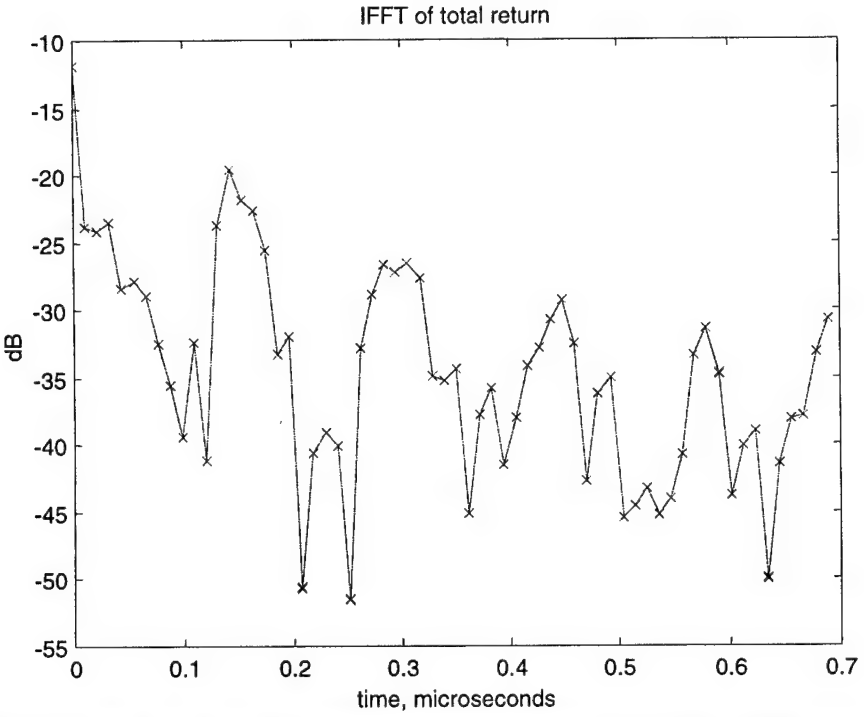

Figure 19: IFFT of the terminal voltages with and without the *x* directed scattering strip (strip at 6m).

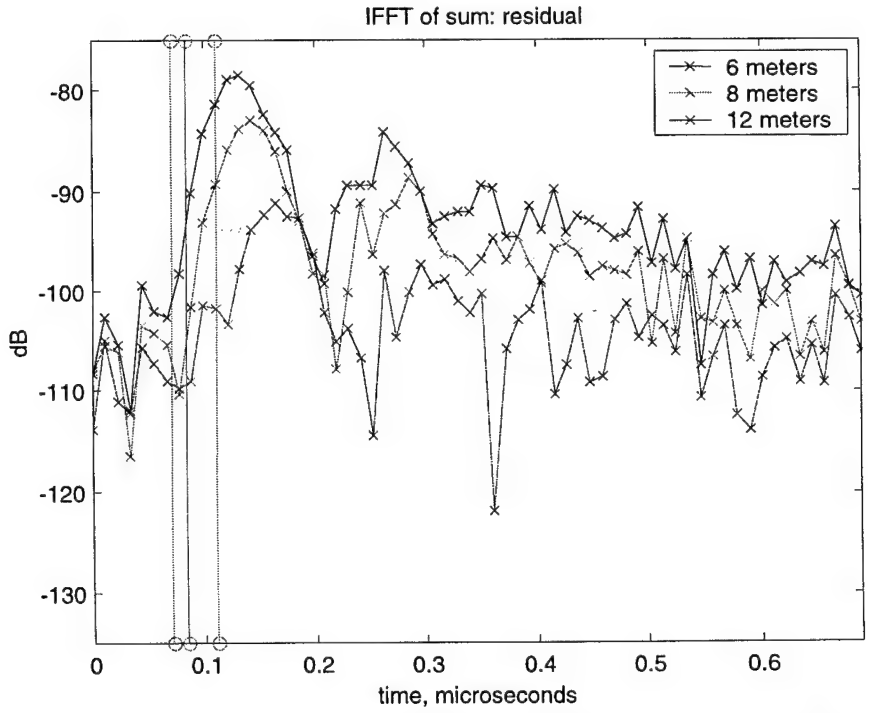

Figure 20: IFFT of the residual voltages with the *x*-directed scattering strip at three distances.

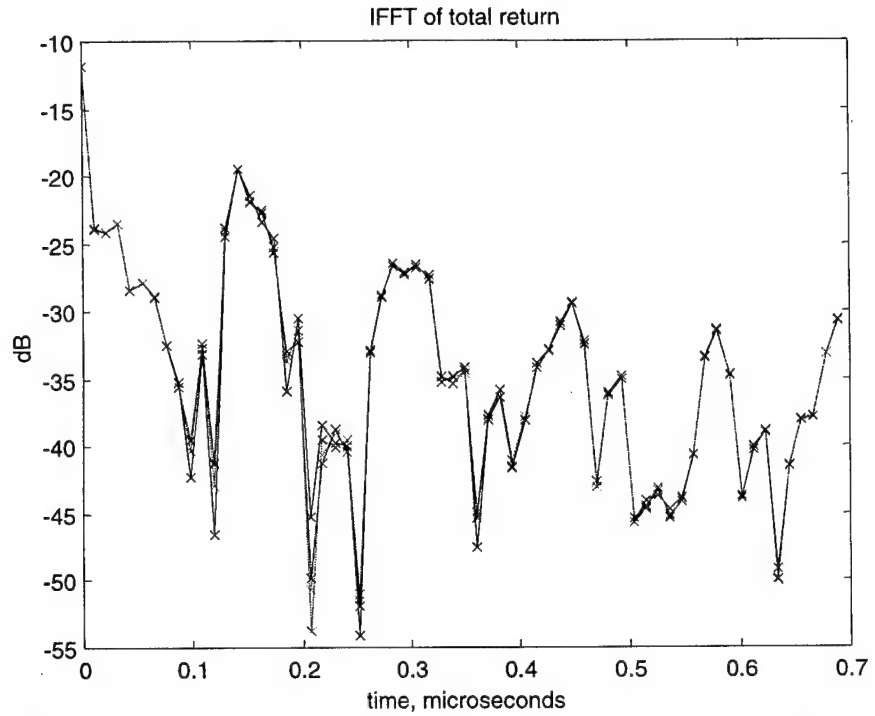

Figure 21: IFFT of the terminal voltages with and without the *y* directed scattering strip (strip at 6m).

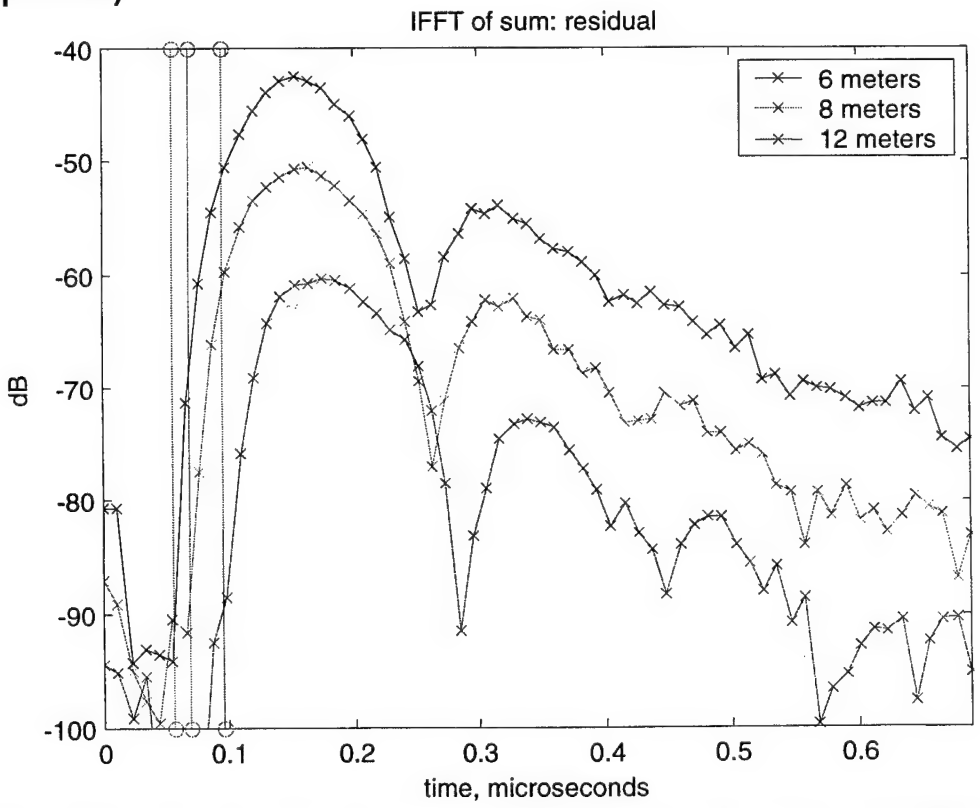

Figure 22: IFFT of the residual voltages with the *y*-directed scattering strip at three distances.

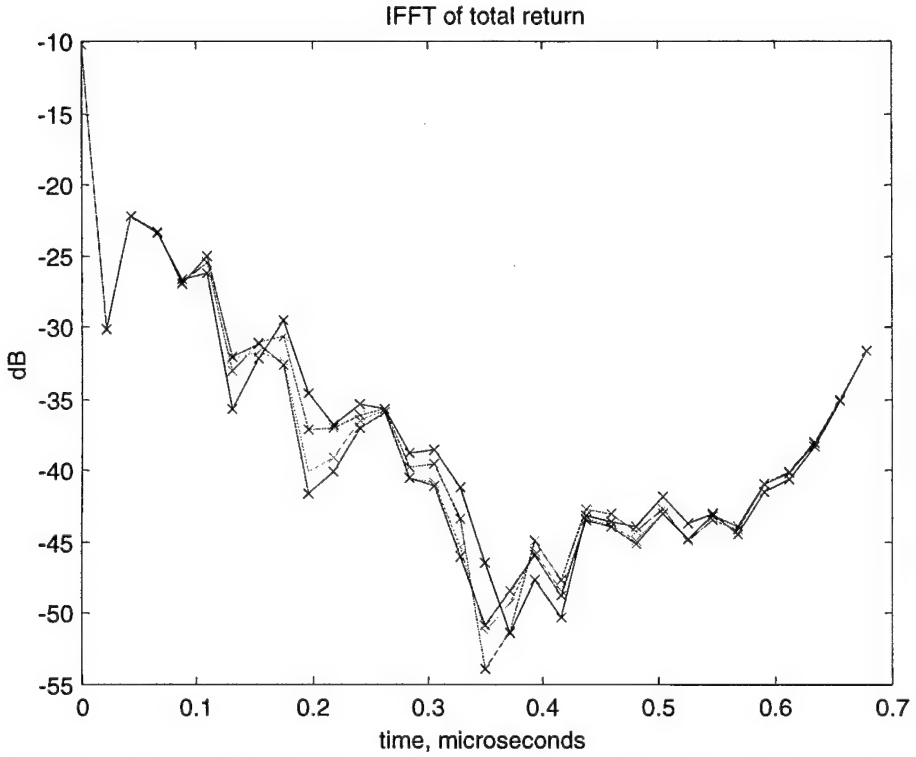

Figure 23: Partial band IFFT of the raw voltages for the disk at three different distances.

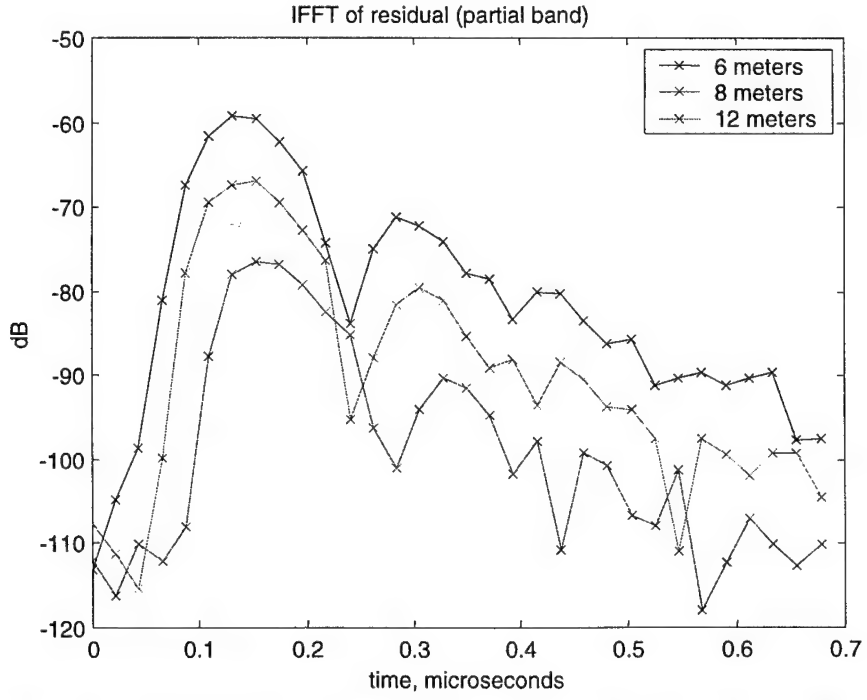

Figure 24: Partial band IFFT of the residual voltages for the disk at three different distances.

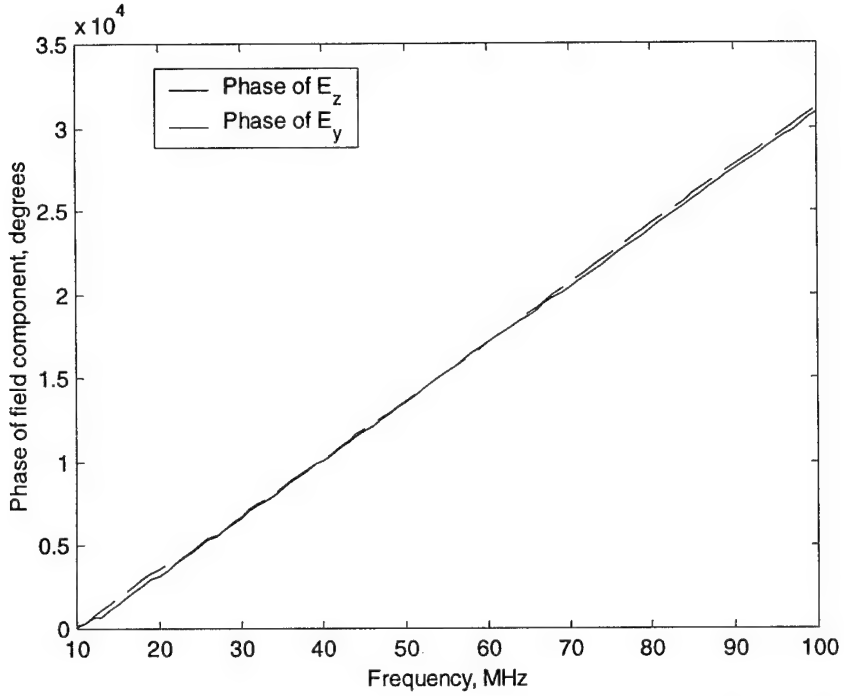

Figure 25: Phase of the *y* and *z* components of the electric field at the point (0,0,6m) as a function of frequency.

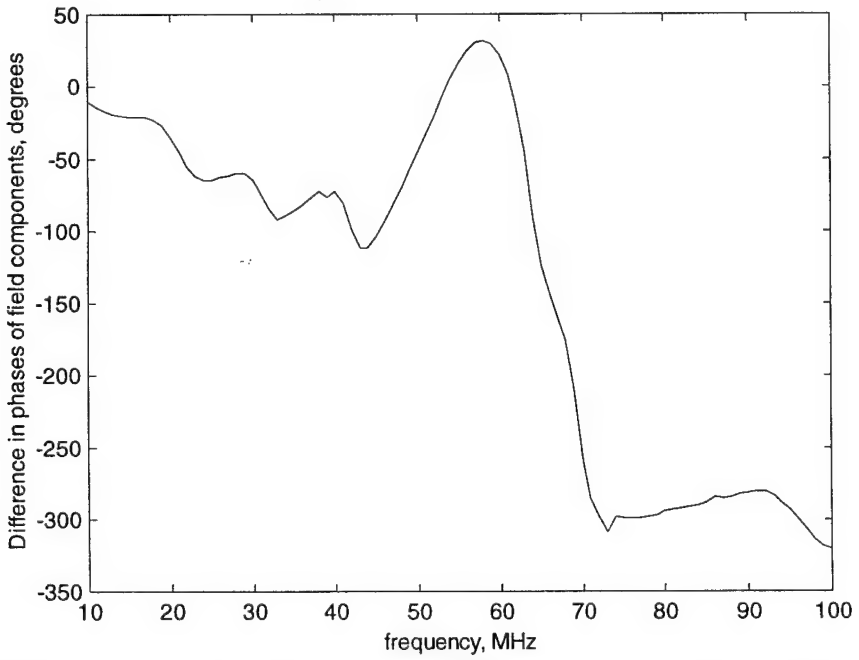

Figure 26: Difference in the phases of the *y* and *z* components of the electric field at the point (0,0,6m) as a function of frequency. The $\exp(-jkR)$ factor is removed.

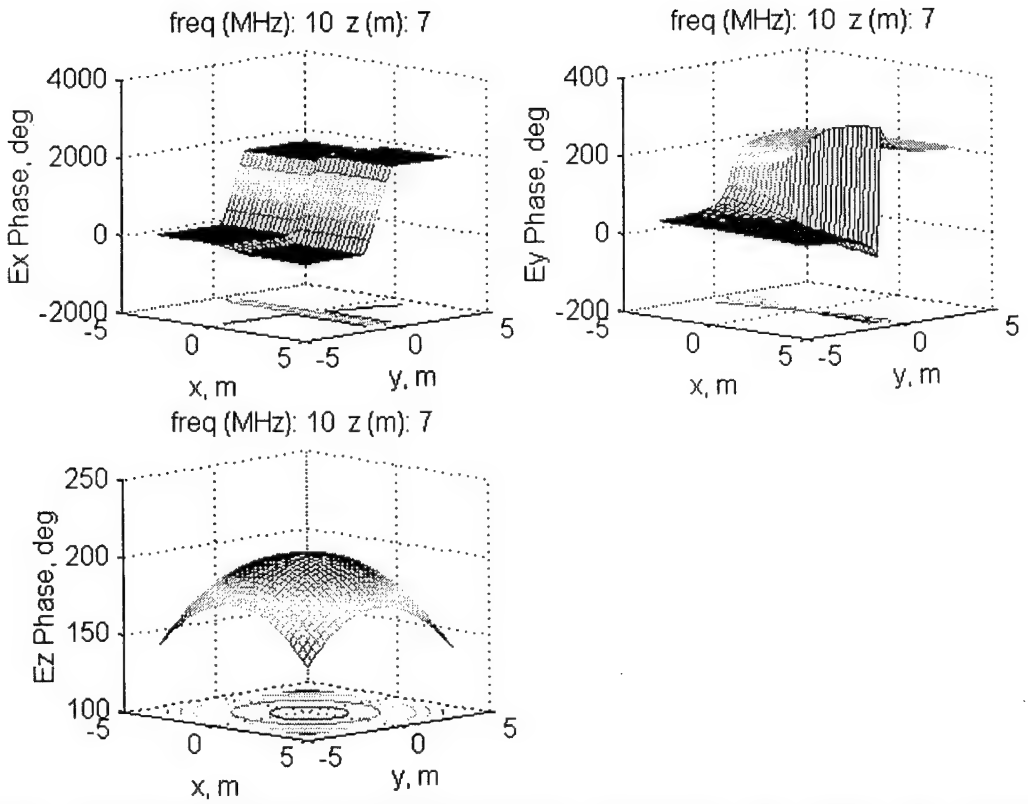

Figure 27: Phase of the field components as a function of *x* and *y* on the plane *z*=7 at 10 MHz.

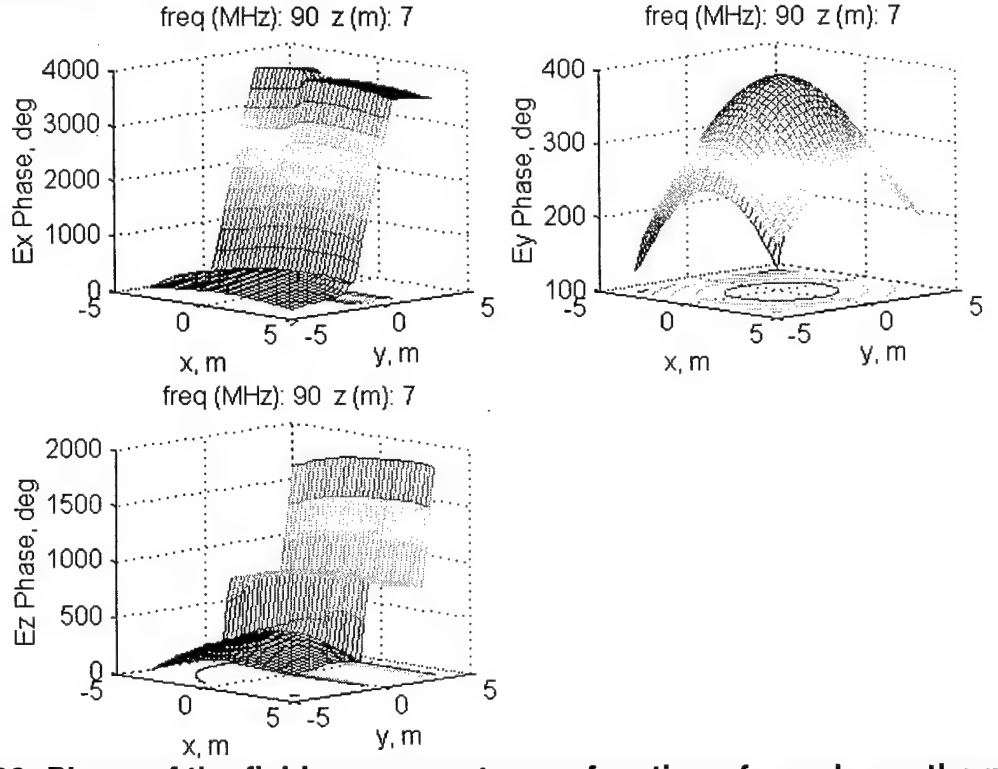

Figure 28: Phase of the field components as a function of *x* and *y* on the plane *z*=7 at 90 MHz.

The reason that the addition of the lower frequencies does not improve the strength of the return is because the phase is changing rapidly with frequency. Figure 25 plots the phase of the z and *y* components of the electric field at the point (0, 0, 6m) as a function of frequency. In Figure 26 the difference between the two is plotted with the $\exp(-jkR)$ factor removed. It is this residual phase error that is degrading the quality of the returns. For complete coherence the difference should be zero at all frequencies. Because the phase error is predictable, it may be possible to compensate for the error in the processing of the returns. Figures 27 and 28 show that the phase is relatively flat throughout the spot area at both 10 MHz and 90 MHz.

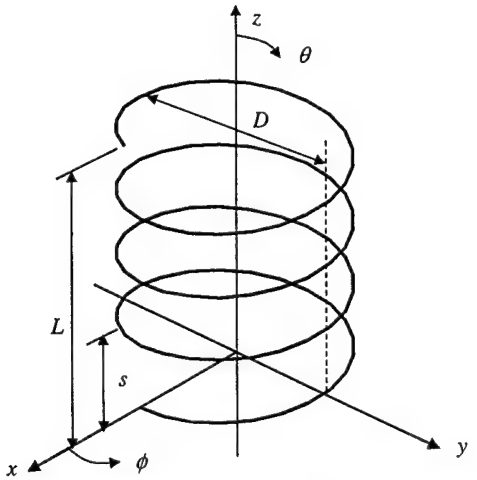

Figure 29: Helix geometry and coordinate system.

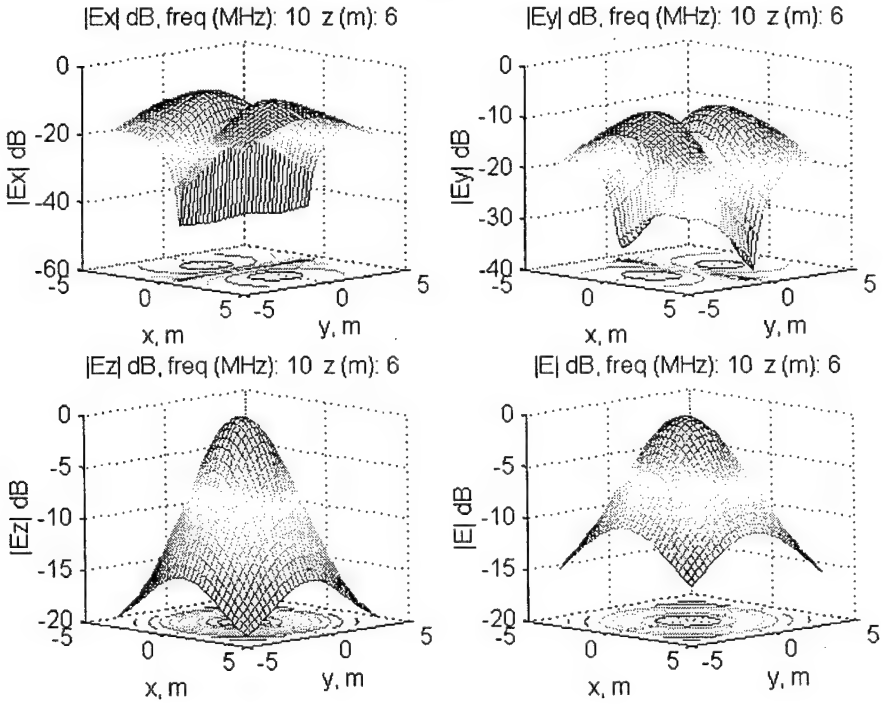

Figure 30: Near field amplitude distribution for a single helix at 10 MHz.

We investigated the suitability of a counter-wound helix as a ground illumination source over the frequency band 10 to 100 MHz. The helix geometry and coordinate system is shown in Figure 29 [1]. A relatively uniform near field illumination spot was obtained over the entire band. However, at lower frequencies in the band, it was found that the axial component of the electric field intensity (E_z) dominated the transverse components (E_x and E_y). An example is shown in Figure 30 for 10 MHz.

The presence of the large *z* component presents problems, because a linearly polarized radiation is desired when a counter winding is added. As shown in Figure 31, for symmetric segments on two counter wound helices the *z* components add on axis. The two segments can be approximated by infinitesimal dipoles that have $E_{\theta'}$ and $E_{r'}$ electric field components, where θ' and r' are defined with respect to each of the dipoles' axis, denoted z'. The components of $E_{\theta'}$ and $E_{r'}$ that lie in the *x-y* plane always cancel for symmetric segments, but the longitudinal parts of these two components always add. Thus some of E_z is due to the $E_{\theta'}$s and some from the $E_{r'}$s.

The *z* components decay rapidly with distance from the helix and generally would not be a problem for observation points in the far field. The θ' and r' components of a dipole do not have the same functional dependence on frequency, and therefore the total E_z is a complicated function of frequency as well as location.

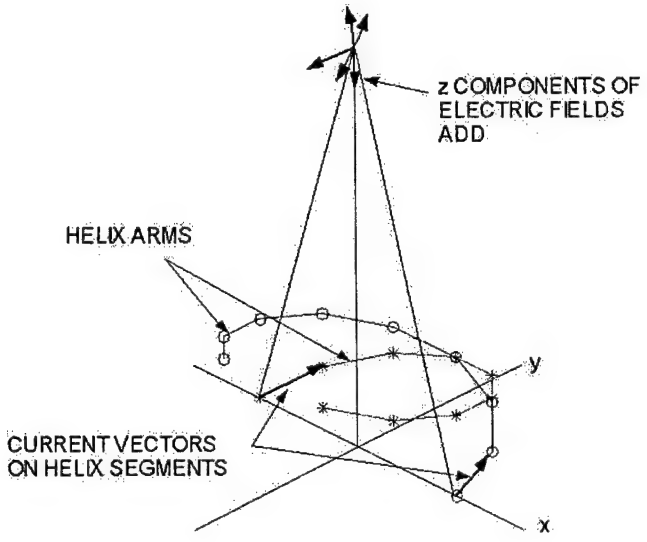

Figure 31: Currents flowing on symmetric segments of a counter wound helices.

Figure 32 plots the phase of the *z* and *y* components of the electric field on axis at a point 2m from the end of the helix as a function of frequency. In Figure 33 the difference between the two phases is plotted with the $\exp(-jkR)$ factor removed. Apparently it is this residual phase error that is degrading the quality of the returns. For complete coherence the difference should be zero at all frequencies.

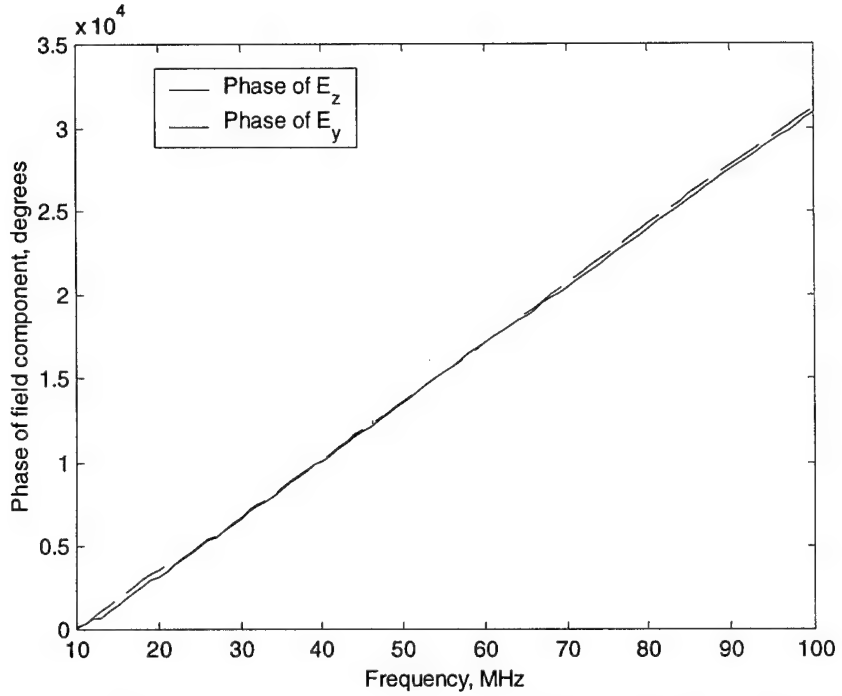

Figure 32: Phase of the *y* and *z* components of the electric field at the point 2m from the end of the helix as a function of frequency.

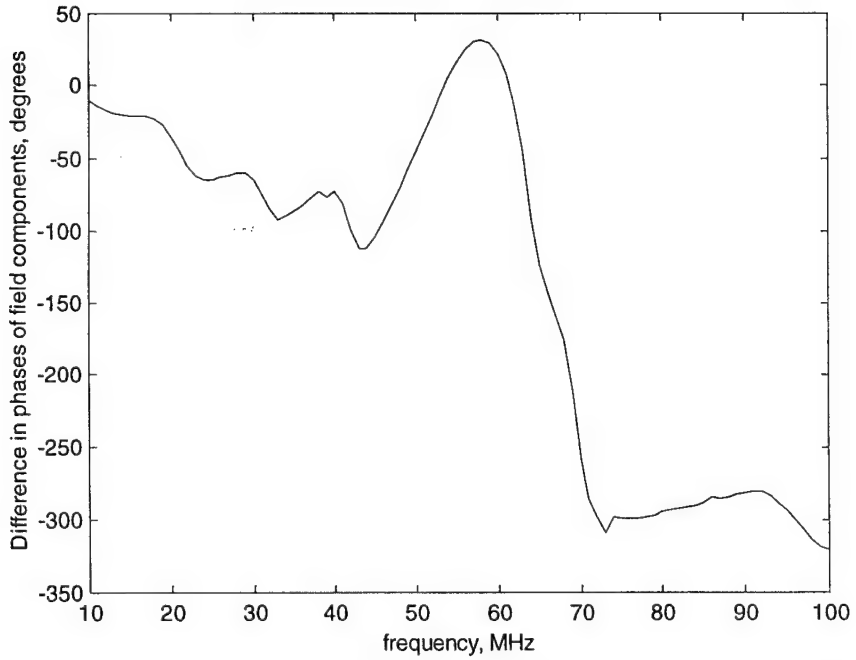

Figure 33: Difference in the phases of the *y* and *z* components of the electric field at a point 2m from the end of the helix as a function of frequency. The $\exp(-jkR)$ factor has been removed.

As illustrated by Figure 34 the phase of the *z* component is relatively flat throughout the spot area at the low frequencies. Because the phase error is predictable, it might be possible to compensate for the error in the processing of the returns. Correction would require a phase weighting that is frequency dependent. As a first iteration, the conjugate of the round trip residual phase difference was used as a correction. This did not improve the quality of the returns, and no further investigation was done along these lines.

From Figure 31 it is clear that if the antenna aperture or elements are restricted to lie in a plane, then the *z* components from symmetric current components will cancel at observation points near the axis. Structures that satisfy this condition are a planar aperture with a TEM aperture field and planar wires. Specifically, a TEM horn and counter wound spirals would yield nearly linear polarized near fields with very small longitudinal field components.

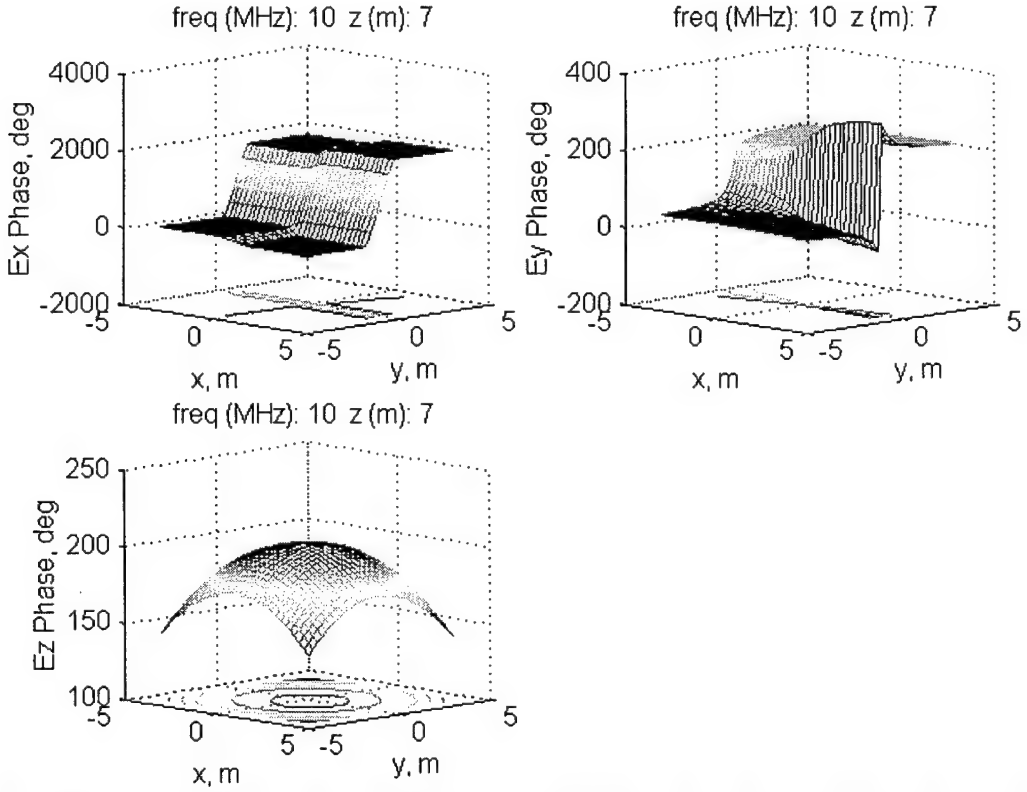

Figure 34: Phase of field components as a function of *x* & *y* on the plane *z*=7 at 10 MHz.

I TEM Horn Antenna

The broad band TEM horn is an old concept [8], and it is commercially available. The major disadvantage is the large size and weight (approximately 75 by 54 by 70 inches for a horn that operates down to 100 MHz). Figure 35 shows a photo of the design described in [8]. The primary application for these horns is electromagnetic compatibility (EMC) testing over wide frequency ranges.

To our knowledge the near field behavior of this type of horn has never been investigated, although it is expected that at observation point near the axis there will be very low longitudinal (normal to the aperture) field components. The approximate near field amplitude is plotted in Figure 36 for 100 MHz assuming that only a tangential aperture field exists. However, an increase in the longitudinal component in the near field can be expected due to:

- nonzero normal aperture current components originating from the feed transition,
- edge currents, and
- currents flowing on the exterior surfaces of the horn.

Although the TEM horn has the required bandwidth and exhibits the proper field behavior, the weight and size are undesirable.

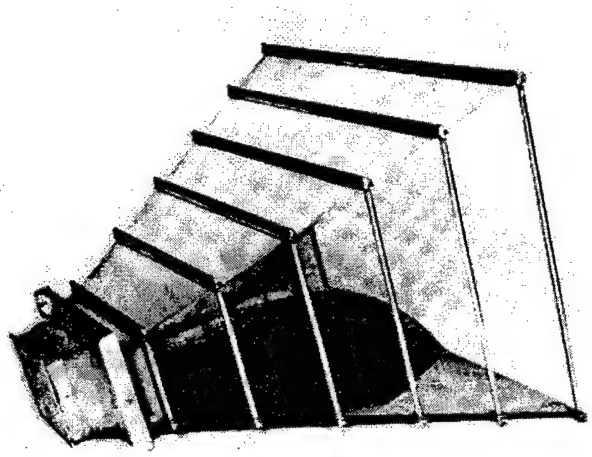

Figure 35: TEM Horn Antenna.

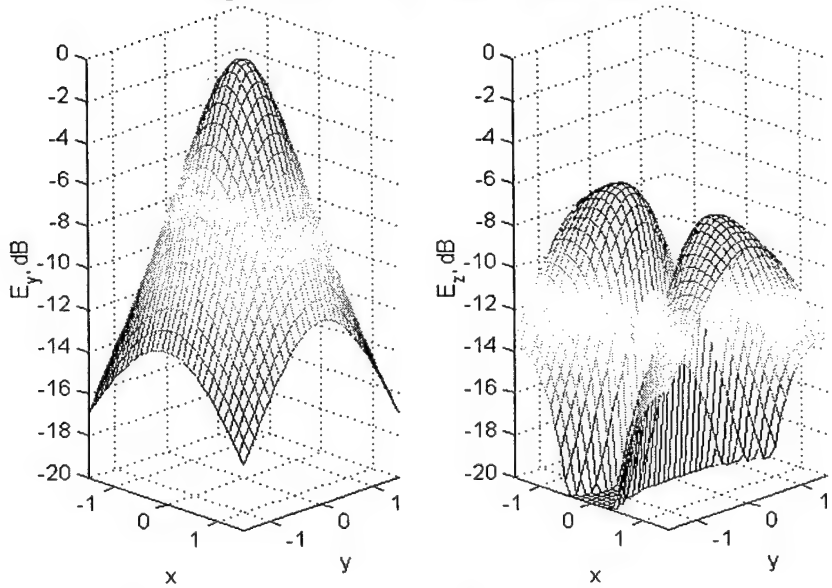

Figure 36: Approximate near field amplitudes of a TEM horn 1m from the aperture at 100 MHz.

J Counter-Wound Spiral Antenna

Another potential solution to the antenna problem is a planar counter-wound spiral antenna. Spirals have demonstrated very wide bandwidths [9]. They are of two general types: Archimedean (circular) or equiangular (logarithmic). The counter-wound concept is illustrated in Figure 37 for the logarithmic spiral. One spiral radiates a left-hand circularly polarized (CP) wave and the second a right-hand CP wave. In principal, combining the outputs yields a linearly polarized wave, with the plane of polarization determined by the phase difference between two feeds. The advantage of this antenna is its flat profile. It will have about the same diameter as the helix, but essentially no depth. In practice, a back plane or cavity will have to be added to provide isolation from objects behind the antenna.

The meshing shown is used for a method of moments program that computes the currents on the spiral arms. The currents are then used to compute the near or far fields. Initial calculations verify that the far-field patterns are linearly polarized. Work is currently under way to calculate the near fields of this antenna. An area of concern is the mutual coupling between the two spirals, which affects both the input impedance and purity of the near field polarization. The method of moments analysis will be capable of predicting the effects of coupling between the two spirals.

At low operating frequencies the spirals are almost linearly polarized. If the two spirals are rotated 90 degrees (rather than 0 degrees, as shown in the figure), two orthogonal polarizations can be obtained by feeding the spirals independently. At high frequencies in the operating band, two orthogonal polarizations can be obtained by feeding the spirals simultaneously with the proper phase difference.

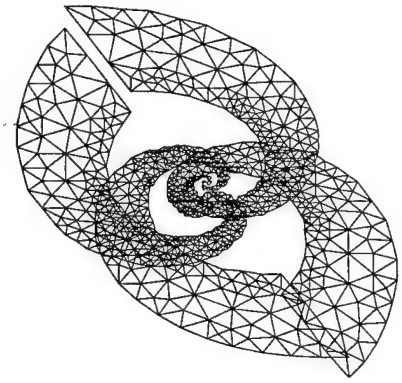

Figure 37: Method of moments mesh model of a counter wound spiral antenna.

An experimental antenna was constructed and tests revealed an unacceptable amount of blockage caused by the overlapping arms of the counter wound spiral.

K SINUOUS ANTENNA

Another potential solution to the antenna problem is a planar sinuous antenna. "In 1983, Randtron Antenna Systems (RAS) developed a common aperture antenna

element with performance equal to or better than a spiral antenna of the same size and capable of simultaneously receiving both senses of circular polarization. This antenna is the Dual Polarized Sinuous Antenna (DPSA). DuHamel and Scherer have published the detailed theory of operation of the DPSA [10]. The DPSAs uniform radiation characteristics are obtained from its radiating aperture. The printed card containing the conductors that carry the currents controlling the radiation is shown on the inset to the right. It consists of two interleaved orthogonal pairs of sinuous-line conductors that are etched onto a dielectric substrate. The dielectric sheet carrying the radiating conductors is mounted above a lossy cavity in a manner similar to a cavity-backed spiral. The cavity forces unidirectional radiation by absorbing the back radiation, which is necessary to maintain control of the antenna patterns and impedance over a broadband. Each conductor pair is excited at the center by a balun that combines opposing conductors in a 0°/180° relationship. These baluns are mounted to the bottom of the lossy cavity and extend into the cavity to connect to the conductors of the etched board.

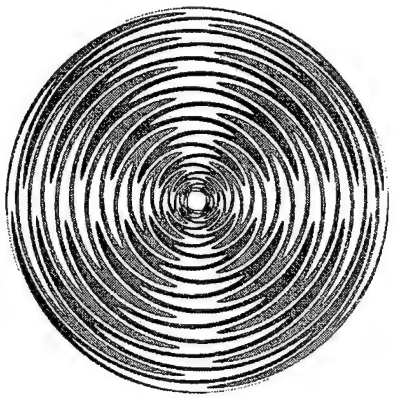

The DPSA has been designed to produce either its latent dual-linear polarization (DLP) or more commonly, in conjunction with a quadrature hybrid, dual-circular polarization (DCP). The DPSA is available with options for dual linear or dual circular polarizations with outputs in individual ports or switch selected into a common port.

For the DCP option, the required quadrature coupler is a very wideband RAS designed stripline 3 dB quadrature hybrid coupler which is specially packaged for DPSA integration. The signals received at each of the dual balun outputs are combined in a ±90° phase relationship by the four port hybrid. The two output ports thus provide right-hand circular polarization (RHCP) and left-hand circular polarization (LHCP) simultaneously. The quality of the circular polarization is measured by the resulting axial ratio (variation in response to rotating linear polarization) which is generally very low over the entire beam.

As an alternate, a dual linearly polarized antenna can be supplied without the quadrature hybrid to provide dual orthogonal linear polarized operation. In the dual linear configuration, it will be shown that the *E*-plane and *H*-plane beamwidths track quite well at all forward angles in space over the frequency band and the *E*-plane and *H*-plane phase centers are coincident. It is this effect that is responsible for the low axial ratio at wide angles in the DCP option. For this reason the DPSA is well suited for use in an EW system application, an interferometer direction finding array, or other applications that require a stable phase center with frequency independent performance."[11]
A comprehensive technical discussion of the sinuous antenna can be found in Dr. R. H. DuHamel patent #4,658,262. Randtron has exclusive rights to this patent.

Randtron built a 15 inch diameter Dual Polarized Sinuous Antenna that covered the frequency band of 0.3 to 6.5 GHz. Nearly a 22:1 bandwidth! The frequency bandwidth limiting factor is the balun and the hybrid. Anzac manufactures a broadband magic T (using discrete components) which covers the frequency band of 2 MHz to 2 GHz, which could be used to feed the antenna. The diameter determines the low frequency cut off with the gain gracefully degrading from 3dBi to -14dBi as shown in the table below.

3 dBi GAIN	-14 dBi GAIN	DIAMETER	DEPTH
100 MHz	50 MHz	48 INCHES	17 INCHES
72 MHz	36 MHz	60 INCHES	23 INCHES
67 MHz	34 MHz	72 INCHES	27 INCHES
57 MHz	29 MHz	84 INCHES	31 INCHES
50 MHz	25 MHz	96 INCHES	36 INCHES
44 MHz	22 MHz	108 INCHES	40 INCHES
40 MHz	20 MHz	120 INCHES	44 INCHES

TABLE 1 DPSA SIZE AND PERFORMANCE BASED ON SCALING

The best antenna candidate is the sinuous dual polarized antenna. The unique feature of the antenna is that it radiates from two localized regions which move outward as the frequency decreases. The lower frequency limit corresponds to the circumference of the circular structure approaching one wavelength; the upper frequency limit is established by the proximity of the central feed arms. The antenna is characterized to a first order by two short dipoles radially displaced from the center by $\lambda/(2\pi)$ thus providing a wide beamwidth of the order of 80 degrees which is independent of frequency. Because the radiating elements form a dual array of closely spaced short dipoles, far-field conditions are obtained in very close proximity to the aperture. This is in contrast with the radiation from conventional aperture antennas which exhibit large dependences of the field distribution as a function of distance from the aperture.

The radiated field distribution observed on a plane separated from the antenna by a distance D (equivalent to height above ground) can be computed by the superposition of fields radiated from the two sources, each weighted in amplitude by the inverse distance between source and observation point and with a phase factor corresponding that distance. The radiating elements are separated by λ/π, and the total field is computed as a function of lateral distance along the ground for different heights.

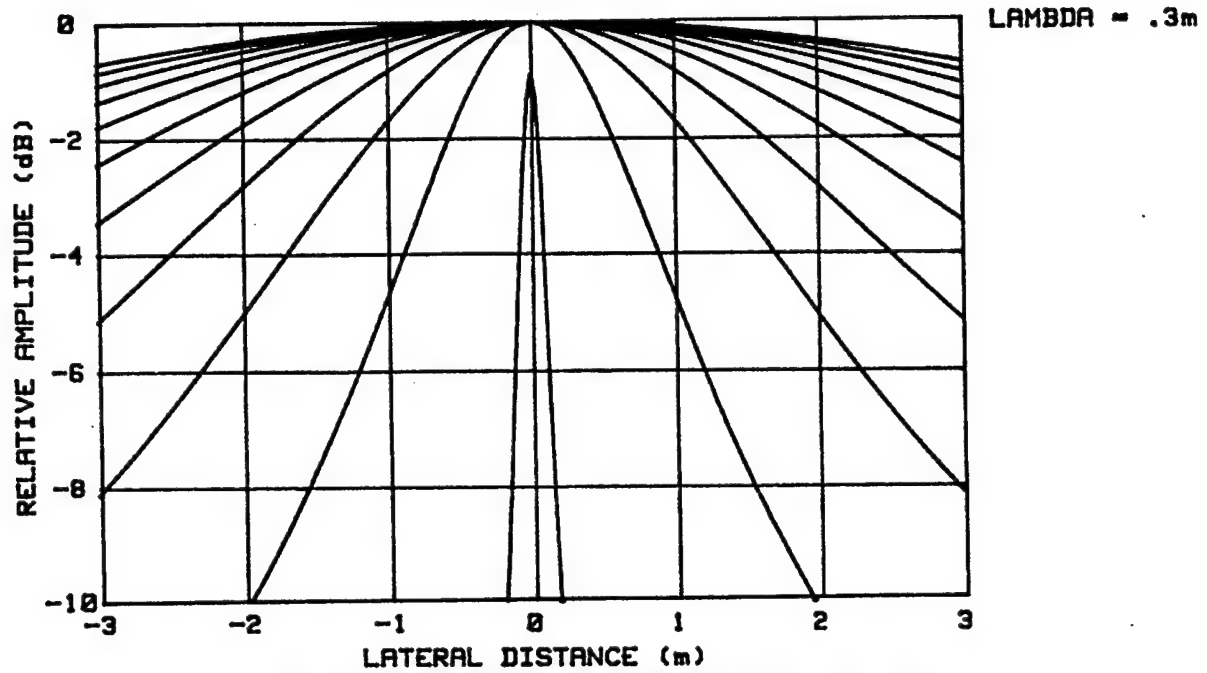

FIGURE 38 RELATIVE AMPLITUDE AT 1 GHz

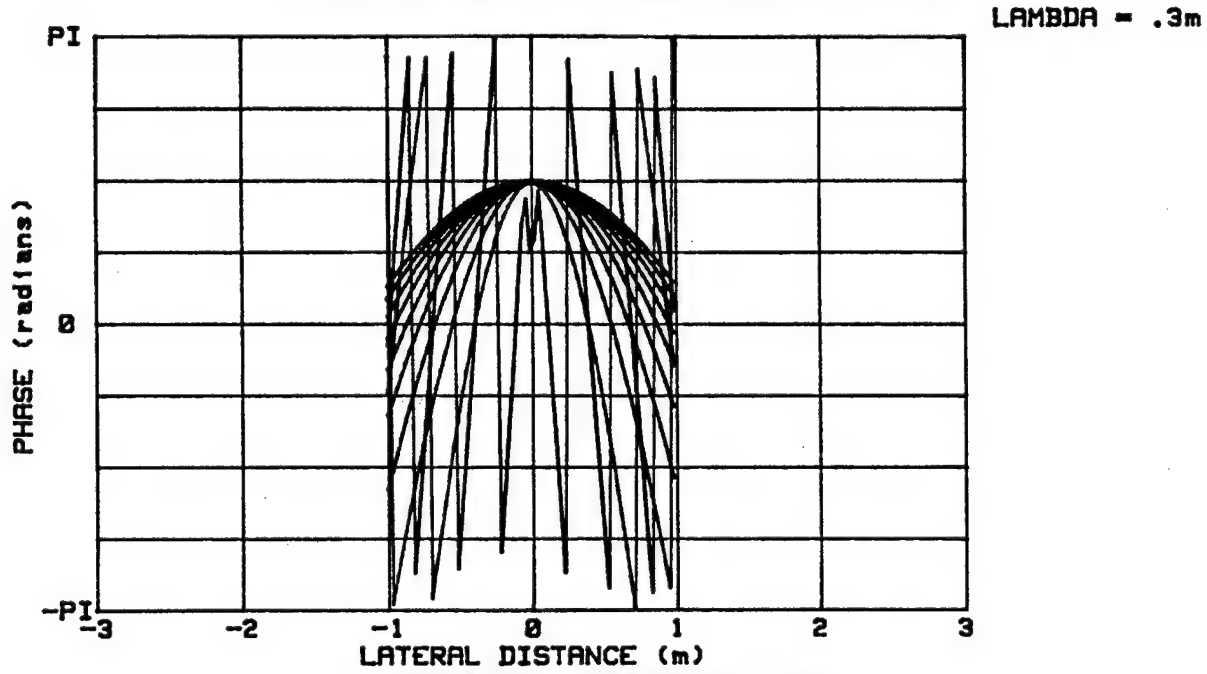

FIGURE 39 PHASE AT 1 GHz

Figures 38, 40, 42, 44 show plots of the field amplitude (shown on the vertical axis) that would be observed along the ground (shown on the horizontal axis) for wavelengths of 0.3, 1, 3, and 5 meters (shown on the legend to the right of the figure). Each figure shows the normalized field amplitude for heights in 1-meter increments. The lowest line corresponds to a distance from the aperture of 0.1 m and the lines progressing upward are for 1 meter increments. The plots indicate that the antenna beam is formed even in close proximity to the aperture.

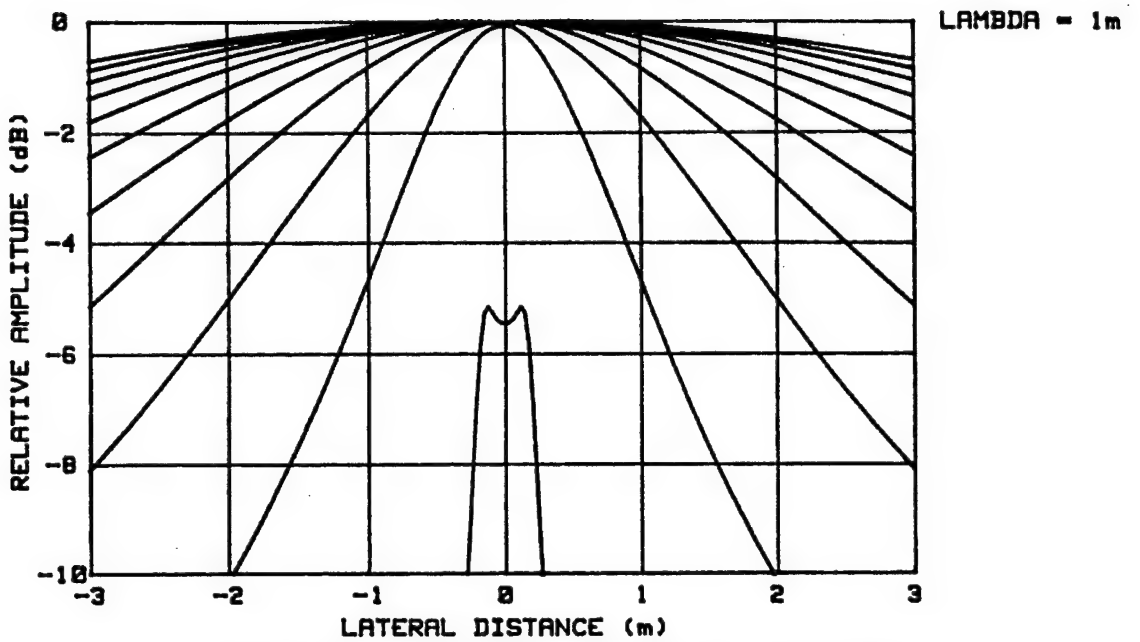

FIGURE 40 RELATIVE AMPLITUDE AT 300 MHz

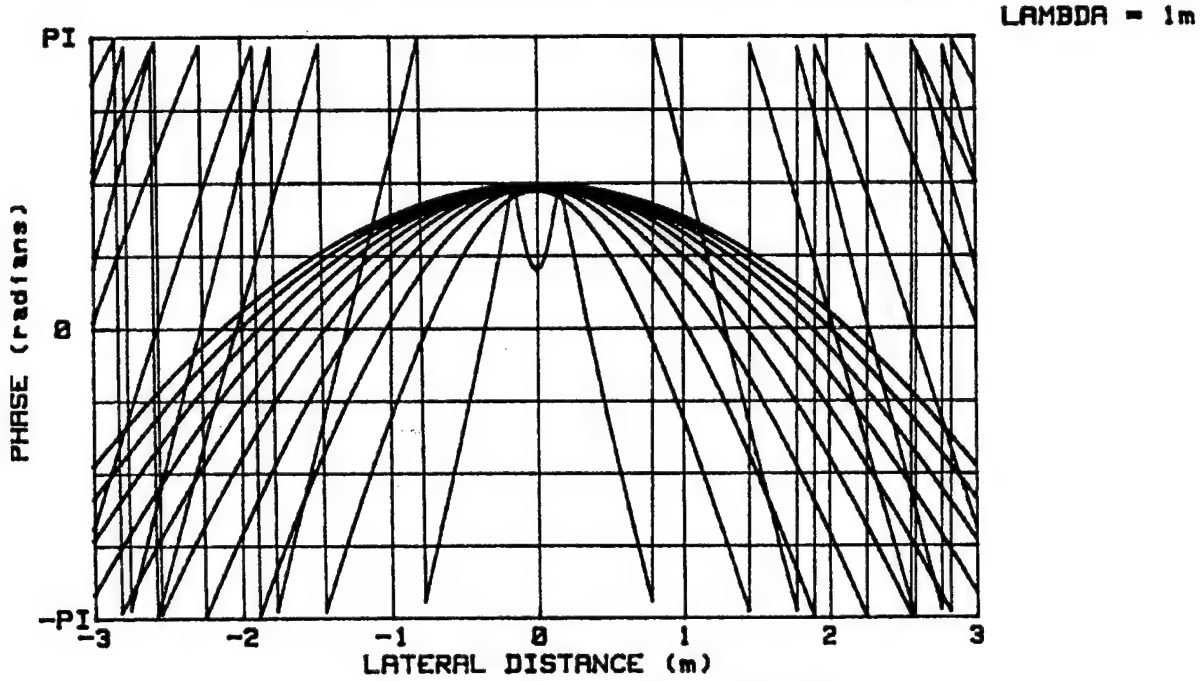

FIGURE 41 PHASE AT 300 MHz

The responses for 0.1 m separation are indicative of the source distribution with the radiating elements separating as the wavelength increases. Figures 39, 41, 43, 45 show the phase of the field for similar conditions. Similar to the amplitude responses, the phase responses show smooth variations. The discontinuities are a consequence of plotting the phase as modulo 2π.

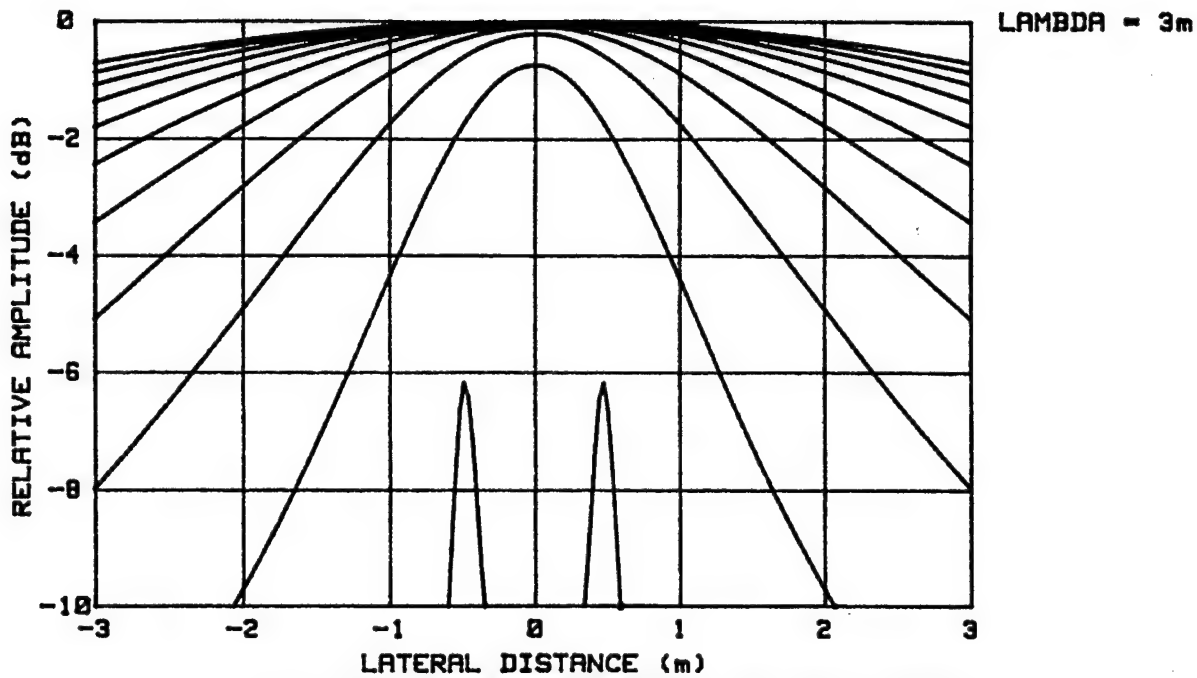

FIGURE 42 RELATIVE AMPLITUDE AT 100 MHz

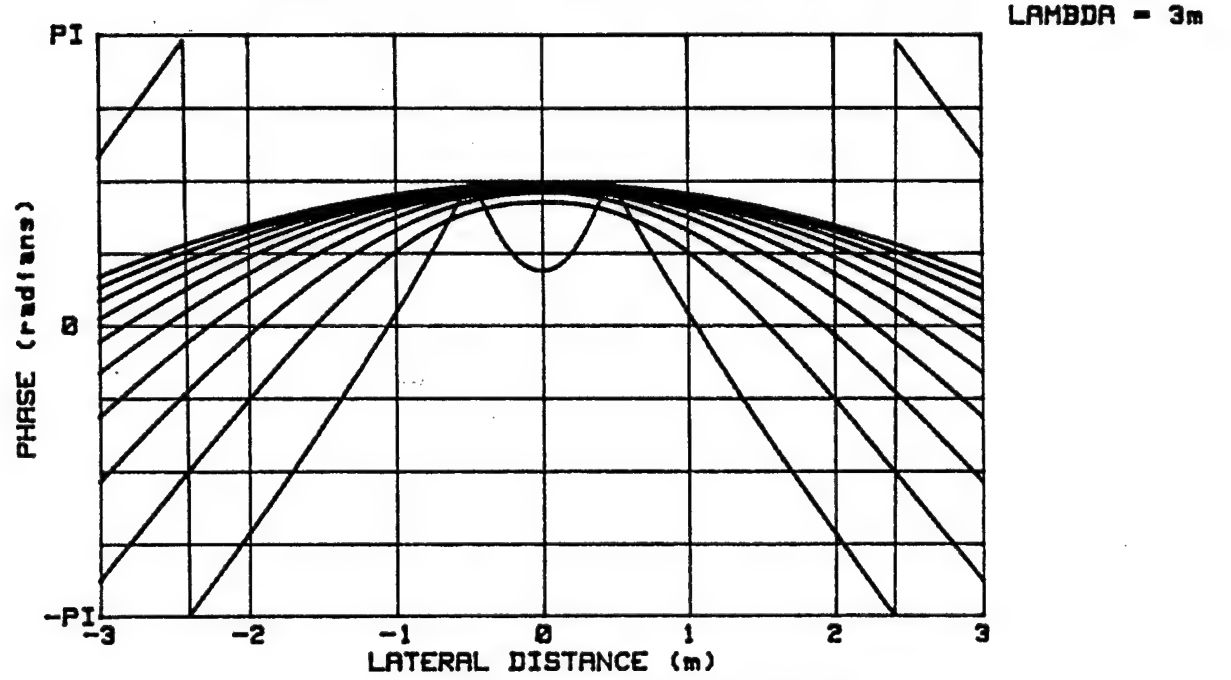

FIGURE 43 PHASE AT 100 MHz

The phase and amplitude responses are consistent with radiation from closely-spaced ($\pi/3$) radiators which behave essentially as a point source. Because of this feature, the antenna achieves far-field conditions in close proximity to the aperture plane, rendering it well suited for this application.

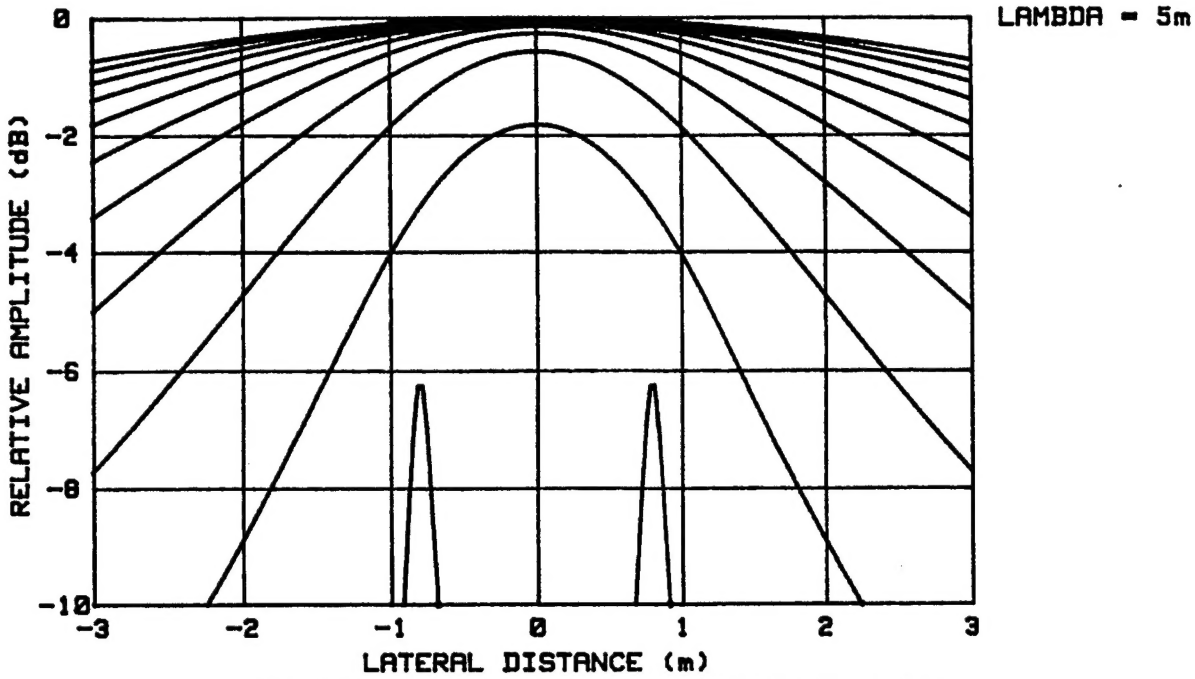

FIGURE 44 RELATIVE AMPLITUDE AT 60 MHz

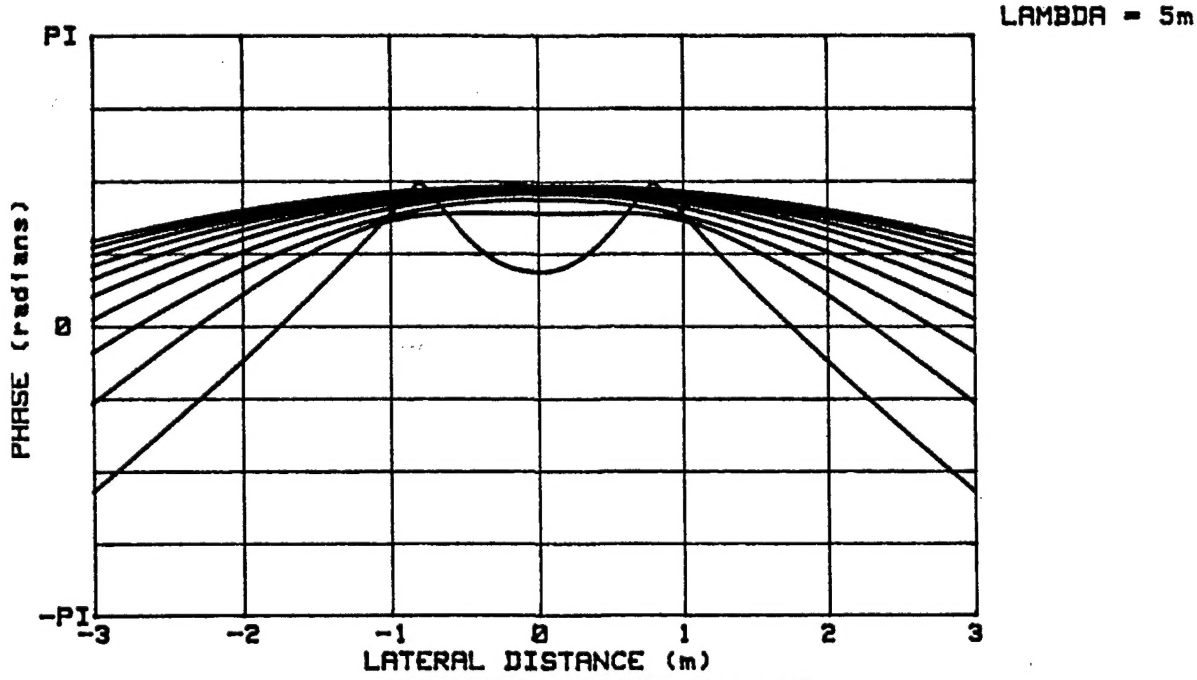

FIGURE 45 PHASE AT 60 MHz

The sinuous antenna provides a significant advantage of achieving far-field conditions very near the aperture plane. The far field distance criterion normally applied is $R = 2D^2/\lambda$ where D is the aperture dimension. In the case of the sinuous antenna, the effective aperture extent is $\tilde{\lambda}/\pi$. Substituting this effective aperture dimension in the far-field relation yields $R = 2\tilde{\lambda}/\pi^2 = 0.2\lambda$ Stutzman and Thiele also cite that for far field to be realized R>>D=wavelength/2 which is 2.5 meters for 60 MHz.

The preceding relation indicates that far-field conditions are achieved in very close proximity to the aperture plane thus rendering the antenna properties useful and predictable at close ranges suitable for GPR applications.

QRC plans in a Phase II contract to issue a contract to Randtron Antenna Systems to build a 48 inch diameter sinuous antenna which is expected to provide useful performance from 50 to 2000 MHz. Randtron will draw upon their experience and consultants to design and build this antenna. As an option, Randtron is willing to build a 100 inch antenna which would provide useful coverage from 25 to 2000 MHz. The near field co and cross polarization performance of the sinuous antenna will be measured on an outdoor near field vertical range which QRC will construct by modifying an existing x-y motor controlled positioning system.

L LOW FREQUENCY RADAR

The Agilent E8356A vector network analyzer is selected for use in the Ground Penetrating Radar. It provides a combination of speed and precision for our needs. This new series has fast sweep speeds, wide dynamic range, low trace noise and flexible connectivity.

Key Features and Specifications

- 256MB RAM
- 300 kHz to 3 GHz
- 128 dB dynamic range at test port
- 143 dB dynamic range with direct receiver access
- 35 µs/point sweep speed
- COM/DCOM and SCPI programming
- TRL/LRM calibration supported
- USB controlled electronic calibration (ECal)
- Source attenuators, bias-tees and direct receiver access standard
- Windows® 2000 operating system

CYCLE TIME (MILLISECONDS)
Start 300 kHz, Stop 3 GHz, 35 kHz IF bandwidth

Number of points	101	201	401	1601
Uncorrected 1 port cal	39	47	56	96
2 port cal	88	101	121	204

Data transfer using a LAN for 1601 points is just 2 milliseconds. Therefore, the collection cycle time for a full 2 port calibrated measurement is 205 milliseconds. This time determines the maximum rate of advance for the GPR. A measurement of every inch of travel should be adequate for detection. Hence, a top speed of 5 inches per second or 300 feet per minute (3.4 mph) is adequate. The speed, of course, will be

determined by the size of targets to be detected. The smaller the target the slower we move.

One of the advantages of this series network analyzer is the configurable test set option where front panel access loops are provided to the signal path between the source output and coupler input. 35 dB step attenuators (5 dB steps) are also added in the receiver paths of both ports. This capability provides the ability to add components or other peripheral instruments for a variety of measurement applications or to make high dynamic range measurements with two-port calibration. Add external power amplifier(s) between the source output and coupler input to provide up to +30 dBm of power at the test port(s). Full two-port error correction measurements are possible. When the DUT output is expected to be less than +30 dBm, measure directly at the B input and use the internal step attenuators to prevent damage to the receiver.

The AMPLIFIER RESEARCH Model 10W1000C covering 500 kHz-1000 MHz is selected as the power amplifier for use with the network analyzer. This amplifier is rated conservatively at 10 watts. It will be working in the 2 watt output region when connected to the NWA. Two watts input to the NWA is the maximum power acceptable to the NWA without damage to the internal coupler. The AR Model 10W1000C is a portable, self-contained, air-cooled, broadband, solid state amplifier designed for applications where instantaneous bandwidth and high gain are required. Push-pull circuitry is utilized in the high power stages to lower distortion and improve stability. A front panel gain control permits the operator to conveniently set the desired output level. The 10W1000C is protected from RF input overdrive by limiting diodes and an RF input leveling circuit which controls the RF input level to the RF amplifier first stage whenever the RF input level is increased above 0 dBm. The RF Amplifier stages are protected from over temperature by removing the DC voltage to them whenever an over temperature condition occurs due to cooling blockage or fan failure. A digital display on the front panel indicates the operational status and fault conditions when an over temperature, power supply, or amplifier fault has occurred. The 10W1000C includes digital control for both local and remote control of the amplifier. This 8-bit RISC microprocessor controlled board provides both IEEE-488 (GPIB) and asynchronous, full duplex RS-232 control of all amplifier functions. The unit weighs 20.5 kg (45.0 lb) and measures 19.8 x 6.1 x 14.8 inches.

Two amplifiers will be configured with the NWA, one for port 1 and the other for port 2. The NWA has provisions to place limiters between the output of the coupler and the input to the receiver. A survey of wideband limiters will be performed to identify a suitable component.

Although in the GPR operating mode the NWA will be used exclusively for data collection and data transfer, the time domain option for the NWA will be purchased. It will provide a method to collaborate the time domain response that is calculated by the system computer.

M SUMMARY

The basic properties of several types of helix antennas have been examined, particularly with regard to their behavior in the near field. At lower frequencies in the band, it was found that the axial component of the electric field intensity (E_z) dominated the transverse components (E_x and E_y). A simulation of scattering from near-field objects in free space demonstrates that there is a measurable return that can be used to generate a down-range coordinate for an image. The phase versus frequency plot for points in the near field begins to oscillate below about 50 MHz. Therefore, coherence is lost and the buildup in signal strength is nowhere near optimal. Helix and conical spirals were rejected for this application.

Horns were evaluated and determined to be too large to be practical to satisfy the low frequency requirement.

The Sinuous antenna was evaluated and selected as the best solution for this application. A dual polarized antenna that can cover the required band of 50 MHz to 2.0 GHz (diameter = 50 inches) or 25 MHz to 2.0 GHz (diameter = 100 inches). Far field behavior at λ/2 height above the ground with the antenna pattern of a 2 element array can be achieved by a wideband sinuous antenna to produce a fully mobile, broadband radar system with a focused planar beam over approximately 20 MHz to 2000 MHz for detection of frozen or thawed layers and the detection of buried objects.

N References

[1] J. D. Kraus, "The Helical Antenna," *Proceedings of the IRE*, vol. 37, no. 3, March 1949, pp. 263-272.

[2] A. Adams and C. Lumjiak, "Optimization of the Quadrifilar Helix Antenna," *IEEE Transactions on Antennas and Propagation*, AP-19, no. 4, July 1971, pp. 547-548.

[3] A. Adams, R. Greenough, R Wallenberg, and C. Lumjiak, *The Quadrifilar Helix Antenna*, Syracuse University Research Corporation report (report number and date unknown; copy available upon request).

[4] W. Johnson, D. Wilton, and R. Sharpe, *Patch Code Users' Manual*, Sandia Laboratory Report SAND87-2991, May 1988.

[5] C. Balanis, *Antenna Theory*, Wiley, 1982.

[6] *Broadband Quasi-Taper Helical Antennas*, The Aerospace Corp., Report SAMSO-TR-77-172, September 1977.

[7] *Characteristics of 5 to 35 Turn Uniform Helical Antennas*, The Aerospace Corporation, Report SAMSO-TR-77-200, June 1977.

[8] J. L. Kerr, "Short Axial Length Broad-Band Horns," *IEEE Trans. on Antennas and Prop.*, vol. AP-21, pp. 710-715, Sept. 1973.

[9] J. Thaysen, K. Jakobsen and J. Appel-Hansen, "A Logarithmic Spiral Antenna for 0.4 to 3.8 GHz," *Applied Microwave & Wireless*, Feb. 2001, p. 32.

[10] Johnson, R.C., editor, *Antenna Engineering Handbook*, third edition, McGraw-Hill Book Company, New York, 1993, chap. 14, pp. 14-53 to 14-62.

[11] L-3 Communications Randtron Antenna Systems Brochure "*The Dual Polarized Sinuous Antenna*", 2002